Mixed Displacement and Couple Stress Finite Element Method for Anisotropic Centrosymmetric Materials

Akhilesh Pedgaonkar[a], Bradley T. Darrall[a], Gary F. Dargush[a,*]

[a]*Department of Mechanical and Aerospace Engineering, University at Buffalo, State University of New York, Buffalo, NY 14260, USA*

Abstract

The classical theory of elasticity is an idealized model of a continuum, which works well for many engineering applications. However, with careful experiments one finds that it may fail in describing behavior in fatigue, at small scales and in structures having high stress concentration factors. Many size-dependent theories have been developed to capture these effects, one of which is the consistent couple stress theory. In this theory, couple stress μ_{ij} is present in addition to force stress σ_{ij} and its tensor form is shown to have skew symmetry. The mean curvature κ_{ij}, which is defined as the skew-symmetric part of the gradient of rotations, is the correct energy conjugate of the couple stress. This mean curvature κ_{ij} and strain e_{ij} together contribute to the elastic energy. The scope of this paper is to extend the work to study anisotropic materials and present a corresponding finite element method. A fully displacement based finite element method for couple stress elasticity requires C^1 continuity. To avoid this, a mixed formulation is presented with primary variables of displacements u_i and couple stress vectors μ_i, both of which require only C^0 continuity. Centrosymmetric classes of materials are considered here for which force stress and strain are decoupled from couple stress and mean curvature in the constitutive relations. Details regarding the numerical implementation are discussed and the effect of couple stress elasticity on anisotropic materials is examined through several computational examples.

Keywords: Consistent Couple Stress Theory, Mixed Variational Formulation, Finite Element Method, Anisotropic Materials, Centrosymmetric Materials

1. Introduction

Classical continuum mechanics predicts the behavior of structures under loads reasonably well at macro scale, but careful experiments have shown that it deviates in capturing behavior of materials at micro scale. Molecular mechanics theory can be used to capture these small scale behaviors but is too computationally intensive to use for practical applications. Hence many size dependent continuum mechanics theories were developed in the past to bridge the gap between problems in the classical and molecular regimes. In classical elasticity theory, forces are transmitted at an infinitesimal element surface as tractions or more specifically force tractions. On the other hand, in size dependent theories, moments are transmitted on an infinitesimal element surface as moment or couple tractions in addition to force tractions. These force and moment tractions can then be represented by tensorial (force) stresses and couple stresses on infinitesimal element. Correspondingly new measures of deformation, such as curvatures, are introduced in addition to strains.

Couple stresses were first proposed by Voigt (1887), but the first mathematical model was presented by Cosserat and Cosserat (1909). Displacements and independent rotations, known as microrotations, were used as the kinematical quantities. Their work was further revived by Mindlin (1964), Eringen (1999), Nowacki (1986) and Chen and Wang (2001). These theories are popularly known today as the micropolar theories.

*corresponding author

Email addresses: apedgaon@buffalo.edu (Akhilesh Pedgaonkar), bdarrall@buffalo.edu (Bradley T. Darrall), gdargush@buffalo.edu (Gary F. Dargush)

Another branch of theories, known as second gradient or strain gradient theories were developed by Mindlin and Eshel (1968), Yang et al. (2002) and Lazar et al. (2005). These involve gradients of strains, rotations and their various combinations all originating from the displacement field to avoid the microrotations.

One other branch of theories based on Voigt (1887) was developed by Toupin (1962), Mindlin and Tiersten (1962) and Koiter (1964) in which displacements and macrorotations were taken as the kinematical quantities. These macrorotaions are the continuum mechanical rotations, which are defined as one half the curl of displacements. Finally the curvatures are defined as gradient of these macrorotations. But these theories had some indeterminacy in the couple stress and force stress tensors due to the limited number of relations. Recently, Hadjesfandiari and Dargush (2011) resolved this indeterminacy and showed the couple stress tensor to be skew symmetric. Furthermore, the mean curvature tensor, which is the skew symmetric part of the gradient of macrorotations, is shown to be the correct energy conjugate of couple stress Hadjesfandiari and Dargush (2011).

In the past few years, there has been an increasing use of macro-rotation-based couple stress theories. Most of the applications are based on Yang et al. (2002), which also is known as modified couple stress theory. Romanoff and Reddy (2014) did an experimental study of web core sandwich panels and compared results with modified couple stress theory for macro-scale Timoshenko beams. Mohammadi et al. (2017) studied the effect of modified couple stress theory on conical nanotubes and compared results with molecular dynamics simulations. Tan and Chen (2019) carried out size-dependent electro-thermo-mechanical analysis of multilayer cantilever microactuators by Joule heating using modified couple stress theory. Lata and Kaur (2019a,b) studied deformation in a transversely isotropic thermoelastic medium using new modified couple stress theory, more closely related to the skew-symmetric couple stress theory. In addition, there has been increasing direct use of consistent couple stress theory by Hadjesfandiari and Dargush (2011). For example, Li et al. (2014) carried out analysis on three-layer microbeams, including electromechanical coupling using consistent couple stress theory, while Dehkordi and Beni (2017) studied electromechanical free vibration of single-walled piezoelectric/flexoelectric nano cones using consistent couple stress theory and compared it with molecular dynamics simulations. Patel et al. (2017) presented simple moment-curvature approach for large deflection analysis of microbeams using consistent couple stress theory. Subramaniam and Mondal (2020) studied the effect of couple stresses on the rheology and dynamics of linear Maxwell viscoelastic fluids. It is important to note that modifed couple stress theory and consistent couple stress theory become equivalent for beam and in-plane deflection problems. According to best of our knowledge, there is no proper experimental validation of any particular theory. In any case, the debate on correctness of theories is beyond the scope of the present paper, as the current work deals with the development of an effective computational method to study the effect of skew-symmetric couple stress in anisotropic materials.

In this present work, a finite element method based on the skew symmetric couple stress theory Hadjesfandiari and Dargush (2011) is developed. This couple stress theory is a fourth order theory. Upon creating the variational formulation, we are left with second order derivatives of displacements. This means a fully displacement based finite element method (FEM) for couple stress theory would require C^1 continuity. To reduce the challenge in maintaining C^1 continuity, three methods have been developed in the past that require at most C^0 continuity. Darrall et al. (2014) defined displacements and rotations as independent variables and then used Lagrange multipliers to constrain these rotations to one half the curl of displacements. Chakravarty et al. (2017) also defined displacements and rotations as independent variables and used penalty parameters to constrain rotations to the displacements. On the other hand, Deng and Dargush (2017) developed a mixed variational formulation with displacements, stresses and couple stresses as independent variables for couple stress elastodynamics. In recent years many developments have been happening in the field of mixed variational methods, which differ from traditional displacement based formulations by including independent variables, such as stresses, strains and surface tractions. The first development can be traced back to the famous Reissner (1950) and Hu (1955); Washizu (1975) principles. Recently, a number of researchers Sivaselvan and Reinhorn (2006); Sivaselvan et al. (2009); Lavan et al. (2009); Apostolakis and Dargush (2011); Lavan (2010); Apostolakis and Dargush (2013) have used mixed variational formulations to solve some interesting and challenging problems in engineering. Also, some analyses of other size dependent theories, namely, micropolar Sachio et al. (1984); Ghosh and Liu (1995); Huang et al. (2000); Providas and Kattis (2002); Li and Xie (2004); Sharbati and Naghdabadi (2006); Riahi and Curran (2009), strain gradient Chen and Wang (2002); Wei (2006) and couple stress Wood (1988); Ma et al. (2008); Reddy (2011) have been done using mixed variational methods.

The method presented in the current work is a mixed formulation based on Deng and Dargush (2017) with a slightly different representation. Here, the novelty involves the use of only two polar (true) vectors, displacement

and couple stress, as primary variables. We apply the resulting stationary principle and finite element method to solve consistent couple stress problems in linear anisotropic elasticity for the first time. For isotropic materials, we have two independent parameters in the constitutive relations between force stresses and strains and one additonal parameter in the couple stress and curvature relations Hadjesfandiari and Dargush (2011). For anisotropic materials, these parameters will be more numerous and interestingly there might be coupling present between force stress - curvatures and similarly in couple stresses - strains. These coupling constitutive relations involve a third order tensor. However, as shown in Nye (1985), a third order tensor has non-zero entries only for non-centrosymmetric materials. Therefore, it is very important to classify materials into centrosymmetric and non-centrosymmetric categories for anisotropic couple stress elasticity. The focus of the current work is restricted to the centrosymmetric category.

The organization of this paper is as follows. An overview of the governing equations, which are required for FEM is presented in Section 2. This basically involves important parts of kinematics, kinetics, boundary conditions and constitutive relations taken from Hadjesfandiari and Dargush (2011). Section 3 concentrates on centrosymmetric materials and incorporates the development of variational formulations. Section 4 then presents the corresponding finite element method. Computational examples are presented in Section 5 to show the effects of this couple stress theory. Finally, in Section 6, conclusions are presented, followed by future work.

2. Governing Equations

This section covers a brief overview of the governing equations from consistent couple stress theory Hadjesfandiari and Dargush (2011) to be used for the current finite element formulations. These equations have been developed for small deformations. Let the volume and surface area of a body under consideration be V and S, respectively.

2.1. Kinematics

Couple stress theory has displacements and macrorotations as kinematical quantities. We present briefly their definitions. Let the displacements be represented by u_i. The gradient of displacement represented by a tensor can be split into symmetric and skew symmetric parts. The first one is known as the strain tensor e_{ij} and the later one as the rotation tensor ω_{ij}. Thus,

$$u_{i,j} = e_{ij} + \omega_{ij} \tag{1}$$

where

$$e_{ij} = \frac{1}{2}(u_{i,j} + u_{j,i}) \tag{2}$$

$$\omega_{ij} = \frac{1}{2}(u_{i,j} - u_{j,i}) \tag{3}$$

Since the rotation tensor is a skew symmetric tensor, it has three independent values and hence can be represented by an axial or pseudo vector. This rotation vector ω_i dual to the rotation tensor is defined according to right hand rule as:

$$\omega_i = \frac{1}{2}\varepsilon_{ijk}\omega_{kj} \tag{4}$$

In terms of displacement it can be represented as:

$$\omega_i = \frac{1}{2}\varepsilon_{ijk}u_{k,j} \tag{5}$$

Here ε_{ijk} is the Levi-Civita symbol or the permutation symbol used in tensor analysis. Note that in classical theory only the strains are considered to induce deformation in a body. Rotations are considered to produce a rigid body motion. It is shown in Hadjesfandiari and Dargush (2011) that, in addition to strain, the skew-symmetric part of gradient of rotations, known as mean curvatures κ_{ij}, is also a fundamental measure of deformation, given by

$$\kappa_{ij} = \frac{1}{2}(\omega_{i,j} - \omega_{j,i}) \tag{6}$$

Again this mean curvature tensor is skew-symmetric and has three independent quantities. Hence it can be represented by a polar vector κ_i or the engineering mean curvature k_i defined in Darrall et al. (2014) as:

$$k_i = -2\kappa_i = \varepsilon_{ijk}\kappa_{jk} = \varepsilon_{ijk}\omega_{j,k} \tag{7}$$

2.2. Kinetics

In couple stress theory Mindlin and Tiersten (1962), couple stresses μ_{ij} are present in addition to force stresses σ_{ij}. The force stress tensor is therefore no longer symmetric and the couple stress tensor is proved to be skew-symmetric. The stress tensor can be split into symmetric $\sigma_{(ij)}$ and skew symmetric part $\sigma_{[ij]}$ as follows.

$$\sigma_{ij} = \sigma_{(ij)} + \sigma_{[ij]} \tag{8}$$

where

$$\sigma_{(ij)} = \frac{1}{2}\left(\sigma_{ij} + \sigma_{ji}\right) \tag{9}$$

$$\sigma_{[ij]} = \frac{1}{2}\left(\sigma_{ij} - \sigma_{ji}\right) \tag{10}$$

Also, since the couple stress tensor μ_{ij} is skew-symmetric, it can be represented by a couple stress vector μ_i as

$$\mu_i = \frac{1}{2}\varepsilon_{ijk}\,\mu_{kj} \tag{11}$$

In this theory, body forces $\hat{f}_i$, force tractions $\hat{t}_i$ and moment tractions $\hat{m}_i$ can exist independently, but body couples are not independent and hence not included in the governing equations. Equilibrium equations for quasi-static couple stress theory from linear and angular momentum balance are given as Hadjesfandiari and Dargush (2011):

$$\begin{aligned} \sigma_{ji,j} + \hat{f}_i &= 0 \\ \varepsilon_{ijk}\,\mu_{k,j} + \varepsilon_{ijk}\sigma_{jk} &= 0 \end{aligned} \tag{12}$$

2.3. Boundary Conditions

In couple stress theory, we have two extra types of boundary conditions with respect to classical elasticity theory making a total of four boundary condition types given below:

$$\begin{aligned} u_i &= \hat{u}_i \text{ on } S_{\hat{u}} \\ \omega_i &= \hat{\omega}_i \text{ on } S_{\hat{\omega}} \\ t_i &= \hat{t}_i \text{ on } S_{\hat{t}} \\ m_i &= \hat{m}_i \text{ on } S_{\hat{m}} \end{aligned} \tag{13}$$

Here u_i are the displacements, ω_i are the tangential rotations as defined in Eq. (5), t_i are the force tractions and m_i are the tangential moment tractions. The quantities having a hat just represents that these are some known values. For a well posed boundary value problem, these surfaces are related as follows:

$$\begin{aligned} S_{\hat{t}} \cup S_{\hat{u}} = S \quad S_{\hat{m}} \cup S_{\hat{\omega}} = S \\ S_{\hat{t}} \cap S_{\hat{u}} = \emptyset \quad S_{\hat{m}} \cap S_{\hat{\omega}} = \emptyset \end{aligned} \tag{14}$$

Also, the above force traction and moment traction can be related to the force stresses and couple stresses, respectively, by the following relations:

$$\begin{aligned} t_i &= \sigma_{ji} n_j \\ m_i &= \varepsilon_{ijk}\,\mu_k n_j \end{aligned} \tag{15}$$

2.4. Constitutive Relations

To relate force stresses and couple stresses to strains and mean curvatures, respectively, we need to define constitutive relations which are given as follows Hadjesfandiari and Dargush (2011):

$$\begin{aligned} \sigma_{(ij)} &= C_{ijkl} e_{kl} + L_{ijk} k_k \\ \mu_i &= D_{ij} k_j + L_{jki} e_{jk} \end{aligned} \tag{16}$$

In the above expression, C_{ijkl} is the constitutive relation tensor between force stresses and strains and D_{ij} is the constitutive relation tensor between couple stresses and curvatures. Meanwhile, L_{ijk} tensor relates force stress to curvatures and couple stresses to strains and is only non-zero for non-centrosymmetric materials. For centrosymmetric materials, the relations above simplify to

$$\begin{aligned} \sigma_{(ij)} &= C_{ijkl} e_{kl} \\ \mu_i &= D_{ij} k_j \end{aligned} \tag{17}$$

Note that the stress written above as $\sigma_{(ij)}$ is the symmetric part of the total force stress tensor given in Eq. (9). Also, we write the inverse constitutive relation between curvatures and couple stress as these would be required for the variational formulation in the next section:

$$k_i = B_{ij} \mu_j \tag{18}$$

where

$$B_{ik} D_{kj} = \delta_{ij} \tag{19}$$

with δ_{ij} as the Kronecker delta identity tensor.

3. Variational Formulation

In this section, we will develop a variational formulation with mixed variables in order to reduce continuity requirements in developing a finite element method. We will start by writing out the total potential energy as a function of the displacement u_i. Then, we will express this energy in terms of an other independent variable, which in this case are the couple stress vector components μ_i. The total potential energy is the addition of strain energy $\mathcal{U}$ stored inside the body and the potential energy $\mathcal{V}$ due to the applied forces. Therefore

$$\Pi = \mathcal{U} + \mathcal{V} \tag{20}$$

According to the consistent couple stress theory Hadjesfandiari and Dargush (2011), the strain energy for centrosymmetric materials can be written as:

$$\mathcal{U} = \frac{1}{2} \int_V e_{ij} C_{ijkl} e_{kl} \, dV + \frac{1}{2} \int_V k_i D_{ij} k_j \, dV \tag{21}$$

In consistent couple stress theory, the applied forces on the body are due to the body force, force traction and moment traction. Hence, the potential energy $\mathcal{V}$ due to applied forces can be written as:

$$\mathcal{V} = - \int_V \hat{f}_i u_i \, dV - \int_{S_{\hat{t}}} \hat{t}_i u_i \, dS - \int_{S_{\hat{m}}} \hat{m}_i \omega_i \, dS \tag{22}$$

Substituting Eqs. (21) and (22) to Eq. (20), we obtain

$$\Pi(\boldsymbol{u}) = \frac{1}{2} \int_V e_{ij} C_{ijkl} e_{kl} \, dV + \frac{1}{2} \int_V k_i D_{ij} k_j \, dV - \int_V \hat{f}_i u_i \, dV - \int_{S_{\hat{t}}} \hat{t}_i u_i \, dS - \int_{S_{\hat{m}}} \hat{m}_i \omega_i \, dS \tag{23}$$

Note that the total potential energy given in Eq. (23) is a function of displacements only. Strain e_{ij}, curvatures k_i and rotations ω_i are all dependent terms and will be expressed in terms of displacements. If we proceed with

this displacement based energy statement, we will require C^1 continuous displacements to develop finite elements, because of the presence of second derivatives in the mean curvature. To reduce the continuity requirements, next we add new independent variables. However, we need to make sure that the energy is expressed correctly in terms of these new variables. By this statement we mean that the energy should still lead to all the governing equations, as the Euler-Lagrange equations of the functional. One of the ways that this can be ensured is to add Lagrange multipliers, which apply additional or missing constraints.

We introduce the couple stress vector components μ_i as our new independent variables and express curvatures k_i in terms of these couple stresses. Since we added these new independent variables, we need to constrain the curvatures to relate to couple stresses using the inverse constitutive relation given in Eq. (18) and Lagrange multipliers α_i. We will see that expressing the total potential energy in terms of these two variables will result in C^0 continuity in both displacements and couple stresses. Since there are no independent rotations, and the displacements are C^0 continuous, we will also need to constrain macrorotation defined as curl of displacements given in Eq. (5) to the known rotations $\hat{\omega}_i$ on the boundary. This can be done using another Lagrange multiplier β_i. Hence the mixed potential energy becomes

$$\begin{aligned}\widetilde{\Pi}(\boldsymbol{u},\boldsymbol{\mu},\boldsymbol{\alpha},\boldsymbol{\beta}) = \frac{1}{2}\int_V e_{ij}C_{ijkl}e_{kl}\,dV + \frac{1}{2}\int_V \mu_i B_{ij}\mu_j\,dV - \int_V \hat{f}_i u_i\,dV - \int_{S_{\hat{t}}} \hat{t}_i u_i\,dS - \int_{S_{\hat{m}}} \hat{m}_i\omega_i\,dS \\ + \int_V \alpha_i\left(k_i - B_{ij}\mu_j\right)dV + \int_{S_{\hat{\omega}}} \beta_i\left(\omega_i - \hat{\omega}_i\right)dS\end{aligned} \tag{24}$$

Using the principle of stationary potential energy, we can say

$$\delta\widetilde{\Pi} = \frac{\partial\widetilde{\Pi}}{\partial u}\delta u + \frac{\partial\widetilde{\Pi}}{\partial\mu}\delta\mu + \frac{\partial\widetilde{\Pi}}{\partial\alpha}\delta\alpha + \frac{\partial\widetilde{\Pi}}{\partial\beta}\delta\beta = 0 \tag{25}$$

Applying this to Eq. (24), we obtain

$$\begin{aligned}\int_V C_{ijkl}e_{kl}\delta e_{ij}\,dV + \int_V B_{ij}\mu_j\delta\mu_i\,dV - \int_V \hat{f}_i\delta u_i\,dV - \int_{S_{\hat{t}}} \hat{t}_i\delta u_i\,dS - \int_{S_{\hat{m}}} \hat{m}_i\delta\omega_i\,dS + \int_V \alpha_i\delta k_i\,dV \\ - \int_V \alpha_i B_{ij}\delta\mu_j\,dV + \int_V \left(k_i - B_{ij}\mu_j\right)\delta\alpha_i\,dV + \int_{S_{\hat{\omega}}} \beta_i\delta\omega_i\,dS + \int_{S_{\hat{\omega}}} \left(\omega_i - \hat{\omega}_i\right)\delta\beta_i\,dS = 0\end{aligned} \tag{26}$$

Let us expand the first and sixth terms, as follows:

$$\int_V C_{ijkl}e_{kl}\delta e_{ij}\,dV = \int_V C_{ijkl}e_{kl}\delta u_{i,j}\,dV \tag{27}$$

$$\begin{aligned}\int_V \alpha_i\delta k_i\,dV &= \int_V \alpha_i\varepsilon_{ijk}\delta\omega_{j,k}\,dV \\ &= \int_V \alpha_k\varepsilon_{ijk}\delta\omega_{i,j}\,dV \\ &= \int_S \alpha_k n_j\varepsilon_{ijk}\delta\omega_i\,dS - \int_V \alpha_{k,j}\varepsilon_{ijk}\delta\omega_i\,dV \\ &= \int_{S_{\hat{m}}} \alpha_k n_j\varepsilon_{ijk}\delta\omega_i\,dS + \int_{S_{\hat{\omega}}} \alpha_k n_j\varepsilon_{ijk}\delta\omega_i\,dS \\ &\quad - \int_V \alpha_{k,j}\varepsilon_{ijk}\delta\omega_i\,dV\end{aligned} \tag{28}$$

Substituting the expansion in Eqs. (27) and (28) into Eq. (26) and writing all macrorotations in terms of displacements (i.e. $\omega_i = \frac{1}{2}\varepsilon_{imn}u_{n,m}$)

$$\begin{aligned}
&\int_V C_{ijkl}e_{kl}\delta u_{i,j}\,dV + \int_V B_{ij}\mu_j\delta\mu_i\,dV - \int_V \hat{f}_i\delta u_i\,dV - \int_{S_{\hat{t}}} \hat{t}_i\delta u_i\,dS - \frac{1}{2}\int_{S_{\hat{m}}} \hat{m}_i\varepsilon_{imn}\delta u_{n,m}\,dS \\
&+\frac{1}{2}\int_{S_{\hat{m}}} \varepsilon_{ijk}\alpha_k n_j\varepsilon_{imn}\delta u_{n,m}\,dS + \frac{1}{2}\int_{S_{\hat{\omega}}} \varepsilon_{ijk}\alpha_k n_j\varepsilon_{imn}\delta u_{n,m}\,dS - \frac{1}{2}\int_V \varepsilon_{ijk}\alpha_{k,j}\varepsilon_{imn}\delta u_{n,m}\,dV - \int_V \alpha_i B_{ij}\delta\mu_j\,dV \\
&+\int_V \left(k_i - B_{ij}\mu_j\right)\delta\alpha_i\,dV + \frac{1}{2}\int_{S_{\hat{\omega}}} \beta_i\varepsilon_{imn}\delta u_{n,m}\,dS + \int_{S_{\hat{\omega}}} \left(\frac{1}{2}\varepsilon_{imn}u_{n,m} - \hat{\omega}_i\right)\delta\beta_i\,dS = 0
\end{aligned} \tag{29}$$

Next, let us group similar variational terms to obtain

$$\begin{aligned}
&\int_V \left(C_{ijkl}e_{kl} + \frac{1}{2}\varepsilon_{kmn}\alpha_{n,m}\varepsilon_{ijk}\right)\delta u_{i,j}\,dV + \int_V \left(B_{ij}\mu_j - B_{ij}\alpha_j\right)\delta\mu_i\,dV - \int_V \hat{f}_i\delta u_i\,dV - \int_{S_{\hat{t}}} \hat{t}_i\delta u_i\,dS \\
&-\frac{1}{2}\int_{S_{\hat{m}}} \left(\hat{m}_i - \varepsilon_{ijk}\alpha_k n_j\right)\varepsilon_{imn}\delta u_{n,m}\,dS + \frac{1}{2}\int_{S_{\hat{\omega}}} \left(\beta_i + \varepsilon_{ijk}\alpha_k n_j\right)\varepsilon_{imn}\delta u_{n,m}\,dS + \int_V \left(k_i - B_{ij}\mu_j\right)\delta\alpha_i\,dV \\
&+\int_{S_{\hat{\omega}}} \left(\frac{1}{2}\varepsilon_{imn}u_{n,m} - \hat{\omega}_i\right)\delta\beta_i\,dS = 0
\end{aligned} \tag{30}$$

Now let us expand the first term using the divergence theorem, such that

$$\begin{aligned}
\int_V \left(C_{ijkl}e_{kl} + \frac{1}{2}\varepsilon_{kmn}\alpha_{n,m}\varepsilon_{ijk}\right)\delta u_{i,j}\,dV = &\int_{S_{\hat{t}}} \left(C_{ijkl}e_{kl} + \frac{1}{2}\varepsilon_{kmn}\alpha_{n,m}\varepsilon_{ijk}\right)n_j\delta u_i\,dS \\
&- \int_V \left(C_{ijkl}e_{kl} + \frac{1}{2}\varepsilon_{kmn}\alpha_{n,m}\varepsilon_{ijk}\right)_{,j}\delta u_i\,dV
\end{aligned} \tag{31}$$

Substituting the expansion in Eq. (31) into Eq. (30) and again grouping the similar variational terms, we find

$$\begin{aligned}
&-\int_V \left(\left(C_{ijkl}e_{kl} + \frac{1}{2}\varepsilon_{kmn}\alpha_{n,m}\varepsilon_{ijk}\right)_{,j} + \hat{f}_i\right)\delta u_i\,dV + \int_V \left(B_{ij}\mu_j - B_{ij}\alpha_j\right)\delta\mu_i\,dV \\
&+\int_{S_{\hat{t}}} \left(\left(C_{ijkl}e_{kl} + \frac{1}{2}\varepsilon_{kmn}\alpha_{n,m}\varepsilon_{ijk}\right)n_j - \hat{t}_i\right)\delta u_i\,dS - \frac{1}{2}\int_{S_{\hat{m}}} \left(\hat{m}_i - \varepsilon_{ijk}\alpha_k n_j\right)\varepsilon_{imn}\delta u_{n,m}\,dS \\
&+\frac{1}{2}\int_{S_{\hat{\omega}}} \left(\beta_i + \varepsilon_{ijk}\alpha_k n_j\right)\varepsilon_{imn}\delta u_{n,m}\,dS + \int_V \left(k_i - B_{ij}\mu_j\right)\delta\alpha_i\,dV + \int_{S_{\hat{\omega}}} \left(\frac{1}{2}\varepsilon_{imn}u_{n,m} - \hat{\omega}_i\right)\delta\beta_i\,dS = 0
\end{aligned} \tag{32}$$

The variational terms in Eq. (32) are completely independent and arbitrary, hence the terms associated with each

separate variational quantity should be zero. Therefore,

$$\begin{aligned}
\left(C_{ijkl}e_{kl} + \frac{1}{2}\varepsilon_{kmn}\alpha_{n,m}\varepsilon_{ijk}\right)_{,j} + \hat{f}_i = 0 \qquad & in\ V \\
B_{ij}\mu_j - B_{ij}\alpha_j = 0 \qquad & in\ V \\
\left(C_{ijkl}e_{kl} + \frac{1}{2}\varepsilon_{kmn}\alpha_{n,m}\varepsilon_{ijk}\right)n_j - \hat{t}_i = 0 \qquad & on\ S_{\hat{t}} \\
\hat{m}_i - \varepsilon_{ijk}\alpha_k n_j = 0 \qquad & on\ S_{\hat{m}} \\
\beta_i + \varepsilon_{ijk}\alpha_k n_j = 0 \qquad & on\ S_{\hat{\omega}} \\
k_i - B_{ij}\mu_j = 0 \qquad & in\ V \\
\frac{1}{2}\varepsilon_{imn}u_{n,m} - \hat{\omega}_i = 0 \qquad & on\ S_{\hat{\omega}}
\end{aligned} \tag{33}$$

In the above relations, the second and fifth equations reveal the unknown Lagrange multipliers as written below:

$$\begin{aligned}
\alpha_i &= \mu_i \\
\beta_i &= -\varepsilon_{ijk}\mu_k n_j
\end{aligned} \tag{34}$$

It is interesting to see that both Lagrange multipliers are function of couple stress μ_i and hence do not add any additional independent variable to the energy. Putting these back in Eq. (33), we see that the stationarity of the potential energy satisfies following equations:

$$\begin{aligned}
\left(C_{ijkl}e_{kl} + \frac{1}{2}\varepsilon_{kmn}\mu_{n,m}\varepsilon_{ijk}\right)_{,j} + \hat{f}_i = 0 \qquad & on\ V \\
\left(C_{ijkl}e_{kl} + \frac{1}{2}\varepsilon_{kmn}\mu_{n,m}\varepsilon_{ijk}\right)n_j - \hat{t}_i = 0 \qquad & on\ S_{\hat{t}} \\
k_i - B_{ij}\mu_j = 0 \qquad & on\ V \\
\frac{1}{2}\varepsilon_{imn}u_{n,m} - \hat{\omega}_i = 0 \qquad & on\ S_{\hat{\omega}}
\end{aligned} \tag{35}$$

The first equation imposes linear momentum balance. The second equation imposes the traction boundary conditions. The third equation constrains displacement based mean curvatures to couple stress using the couple stress - curvature constitutive relations. The fourth equation satisfies the rotation boundary conditions on displacements. Note that in this formulation the force stress - strain relations, angular momentum balance and moment traction boundary conditions are satisfied essentially due to the choice of variables. The equations in Eq. (35) will be satisfied variationally or in a weak sense.

Let us return to the total potential energy given in Eq. (24) and substitute the Lagrange multipliers obtained in Eq. (34). After simplifying, we obtain

$$\begin{aligned}
\widetilde{\Pi}(\boldsymbol{u},\boldsymbol{\mu}) = \frac{1}{2}\int_V e_{ij}C_{ijkl}e_{kl}\,dV - \frac{1}{2}\int_V \mu_i B_{ij}\mu_j\,dV + \int_V \mu_i k_i\,dV - \int_V \hat{f}_i u_i\,dV - \int_{S_{\hat{t}}} \hat{t}_i u_i\,dS - \frac{1}{2}\int_{S_{\hat{m}}} \hat{m}_i\varepsilon_{imn}u_{n,m}\,dS \\
- \int_{S_{\hat{\omega}}} \varepsilon_{ijk}\mu_k n_j\left(\frac{1}{2}\varepsilon_{imn}u_{n,m} - \hat{\omega}_i\right)dS
\end{aligned} \tag{36}$$

We see that the potential energy is a function of two independent variables; namely, displacements and couple stresses, which is a unique feature of this formulation. However, curvatures k_i involve the second order derivatives of displacements, which would require C^1 continuity. We again simplify the total potential energy by expanding the third term,

as follows:

$$\begin{aligned}\int_V \mu_i k_i \, dV &= \int_V \mu_i \varepsilon_{ijk} \omega_{j,k} \, dV \\ &= \int_V \mu_k \varepsilon_{ijk} \omega_{i,j} \, dV \\ &= \int_S \varepsilon_{ijk} \mu_k n_j \omega_i \, dS - \int_V \varepsilon_{ijk} \mu_{k,j} \omega_i \, dV \\ &= \frac{1}{2} \int_S \varepsilon_{ijk} \mu_k n_j \varepsilon_{imn} u_{n,m} \, dS - \frac{1}{2} \int_V \varepsilon_{ijk} \mu_{k,j} \varepsilon_{imn} u_{n,m} \, dV \\ &= \frac{1}{2} \int_{S_{\hat{m}}} \hat{m}_i \varepsilon_{imn} u_{n,m} \, dS + \frac{1}{2} \int_{S_{\hat{\omega}}} \varepsilon_{ijk} \mu_k n_j \varepsilon_{imn} u_{n,m} \, dS - \frac{1}{2} \int_V \varepsilon_{ijk} \mu_{k,j} \varepsilon_{imn} u_{n,m} \, dV\end{aligned} \tag{37}$$

Substituting Eq. (37) into Eq. (36) and simplifying, we find

$$\begin{aligned}\widetilde{\Pi}(\boldsymbol{u}, \boldsymbol{\mu}) = \frac{1}{2} \int_V e_{ij} C_{ijkl} e_{kl} \, dV - \frac{1}{2} \int_V \mu_i B_{ij} \mu_j \, dV - \frac{1}{2} \int_V \varepsilon_{ijk} \mu_{k,j} \varepsilon_{imn} u_{n,m} \, dV - \int_V \hat{f}_i u_i \, dV - \int_{S_{\hat{t}}} \hat{t}_i u_i \, dS \\ + \int_{S_{\hat{\omega}}} \varepsilon_{ijk} \mu_k n_j \hat{\omega}_i \, dS\end{aligned} \tag{38}$$

Finally Eq. (38) is an attractive form of the potential energy in terms of the independent variables; namely, displacement and couple stress. Now, at most, only first derivatives are present in Eq. (38).

Taking the variation of above equation we obtain our weak form to be used for the finite element method, as follows:

$$\begin{aligned}\int_V C_{ijkl} e_{kl} \delta e_{ij} \, dV - \int_V B_{ij} \mu_j \delta \mu_i \, dV - \frac{1}{2} \int_V \varepsilon_{ijk} \mu_{k,j} \varepsilon_{imn} \delta u_{n,m} \, dV - \frac{1}{2} \int_V \varepsilon_{imn} u_{n,m} \varepsilon_{ijk} \delta \mu_{k,j} \, dV - \int_V \hat{f}_i \delta u_i \, dV \\ - \int_{S_{\hat{t}}} \hat{t}_i \delta u_i \, dS + \int_{S_{\hat{\omega}}} \hat{\omega}_i \varepsilon_{ijk} n_j \delta \mu_k \, dS = 0\end{aligned} \tag{39}$$

We see that Eq. (39) has two independent variables, namely, the displacement u_i and the couple stress vector μ_i, both of which have highest derivative order of one. Hence both these variables require only C^0 continuity. This mixed displacement and couple stress vector based formulation therefore reduced the original C^1 continuity requirements of a pure displacement based formulation to C^0. The trade-off is that the functional in Eq. (39) leads to a stationary principle, whereas the original formulation expressed in Eq. (23) is associated with a minimum of the functional.

4. Finite Element Formulation

To begin the finite element formulation, we first analyze our weak statement given in Eq. (39). We see that this equation only has two variables, namely, displacement vector u_i and the couple stress vector μ_i, which have each a maximum of first order derivatives. Hence, we need to maintain at least C^0 continuity in both these variables for the finite element method (FEM).

In this present work, a 2D finite element method is presented for the computational examples. We solve plane strain problems, where the deflections are assumed to be in the plane and only depend on planar coordinates. Let the coordinates be x_1, x_2 and x_3 and deflections along these coordinates be u_1, u_2 and u_3, respectively. The coordinates x_1

and x_2 are in the plane, while x_3 is out of the plane. Then,

$$\begin{aligned} u_1 &\equiv u_1(x_1, x_2) \\ u_2 &\equiv u_2(x_1, x_2) \\ u_3 &\equiv 0 \end{aligned} \tag{40}$$

For planar deflections, $\omega_i = \frac{1}{2}\varepsilon_{ijk}u_{k,j}$ yields only one non-zero rotation component $\omega_3 = \omega$. Since the curvature $k_i = \varepsilon_{ijk}\omega_{j,k}$, we only have two non-zero curvatures k_1 and k_2. Correspondingly we will require only two couple stress vector components μ_1 and μ_2 in our finite elements. Note μ_3 might be non-zero, but is not required for the analysis if the constitutive matrix is taken appropriately. Therefore, for the current 2D finite elements only four variables remain, namely, u_1, u_2, μ_1 and μ_2. Four noded quad elements are selected for both the variables with the standard shape functions N where

$$N = \begin{bmatrix} \frac{1}{4}(1-\xi)(1-\eta) \\ \frac{1}{4}(1+\xi)(1-\eta) \\ \frac{1}{4}(1+\xi)(1+\eta) \\ \frac{1}{4}(1-\xi)(1+\eta) \end{bmatrix} \tag{41}$$

These shape functions are used to represent both the coordinates and the variables of an arbitrary element by multiplying with their nodal values. Thus,

$$x_1 = N_\alpha x_1^{(\alpha)} \qquad x_2 = N_\alpha x_2^{(\alpha)} \tag{42}$$

$$\begin{aligned} u_1 &= N_\alpha u_1^{(\alpha)} \qquad & u_2 &= N_\alpha u_2^{(\alpha)} \\ \mu_1 &= N_\alpha \mu_1^{(\alpha)} \qquad & \mu_2 &= N_\alpha \mu_2^{(\alpha)} \end{aligned} \tag{43}$$

with sum over α where $u_1^{(\alpha)}$ and all similar terms are nodal variables, while u_1 and all similar terms are the variable functions. We also define the following arrangements of nodal quantities to be used in the FEM:

$$\begin{aligned} \bar{u} &= \left[u_1^{(1)} u_2^{(1)} \quad ..... \quad u_1^{(4)} u_2^{(4)}\right]^T \\ \bar{\mu} &= \left[\mu_1^{(1)} \mu_2^{(1)} \quad ..... \quad \mu_1^{(4)} \mu_2^{(4)}\right]^T \\ \hat{f} &= \left[\hat{f}_1^{(1)} \hat{f}_2^{(1)} \quad ..... \quad \hat{f}_1^{(4)} \hat{f}_2^{(4)}\right]^T \\ \hat{t} &= \left[\hat{t}_1^{(1)} \hat{t}_2^{(1)} \hat{t}_1^{(2)} \hat{t}_2^{(2)}\right]^T \\ \hat{\omega} &= \left[\hat{\omega}^{(1)} \hat{\omega}^{(2)}\right]^T \end{aligned} \tag{44}$$

where $\hat{t}$ and $\hat{\omega}$ are defined at the two nodes of an element edge. Also note that the quantities with hats are known quantities and hence are not variables.

Putting these arrangements from Eq. (44) and variables defined in terms of nodal variables in Eqs. (42) and (43) back into the weak statement Eq. (39), we obtain

$$-\delta\bar{u}^T[C]\bar{u} + \delta\bar{\mu}^T[B]\bar{\mu} + \delta\bar{u}^T[G]\bar{\mu} + \delta\bar{\mu}^T[G]^T\bar{u} + \delta\bar{u}^T[\hat{F}] + \delta\bar{u}^T[\hat{T}] - \delta\bar{\mu}^T[\hat{\Omega}] = 0 \tag{45}$$

where the square bracketed terms are defined as

$$
\begin{aligned}
[C] &= \int_V Q_e^T C Q_e \, det(J) dV \\
[B] &= \int_V Q_\mu^T B Q_\mu \, det(J) dV \\
[G] &= \frac{1}{2} \int_V Q_\zeta^T Q_\zeta \, det(J) dV \\
[\hat{F}] &= \int_V Q_u^T Q_f \bar{f} \, det(J) dV \\
[\hat{T}] &= \int_{S_{\hat{t}}} Q_v^T Q_t \bar{t} \, det(J_s) dS \\
[\hat{\Omega}] &= \int_{S_{\hat{\omega}}} Q_t^T \hat{n}^T Q_\omega \bar{\omega} \, det(J_s) dS
\end{aligned}
\tag{46}
$$

The terms involving Q with a subscript are defined as

$$
\begin{aligned}
Q_e &= \begin{bmatrix} \frac{\partial N_1}{\partial x_1} & 0 & ..... & \frac{\partial N_4}{\partial x_1} & 0 \\ 0 & \frac{\partial N_1}{\partial x_2} & ..... & 0 & \frac{\partial N_4}{\partial x_2} \\ \frac{\partial N_1}{\partial x_2} & \frac{\partial N_1}{\partial x_1} & ..... & \frac{\partial N_1}{\partial x_2} & \frac{\partial N_1}{\partial x_1} \end{bmatrix} \\
Q_u = Q_\mu = Q_f &= \begin{bmatrix} N_1 & 0 & ... & N_4 & 0 \\ 0 & N_1 & ... & 0 & N_4 \end{bmatrix} \\
Q_\zeta &= \begin{bmatrix} -\frac{\partial N_1}{\partial x_2} & \frac{\partial N_1}{\partial x_1} & ..... & -\frac{\partial N_4}{\partial x_2} & \frac{\partial N_4}{\partial x_1} \end{bmatrix} \\
Q_v = Q_t &= \begin{bmatrix} N_{s_1} & 0 & N_{s_2} & 0 \\ 0 & N_{s_1} & 0 & N_{s_2} \end{bmatrix} \\
Q_\omega &= \begin{bmatrix} N_{s_1} & N_{s_2} \end{bmatrix} \\
\hat{n} &= \begin{bmatrix} -n_2 & n_1 \end{bmatrix}
\end{aligned}
\tag{47}
$$

The terms N_1, N_2, ... in above expressions are the shape functions given in Eq. (41) and the terms N_s are the shape functions used to apply boundary conditions. These surface based shape functions are defined on the edge of a quadrilateral element present at the boundary as:

$$
N_s = \begin{bmatrix} \frac{1}{2}(1-\xi) \\ \frac{1}{2}(1+\xi) \end{bmatrix} \tag{48}
$$

In Eq. (46), the term J is the jacobian of an element, while J_s is the jacobian of the edge of an element, which lies on the boundary of the body. For linear shape functions, these are defined as:

$$
J = \begin{bmatrix} \frac{\partial x_1}{\partial \xi} & \frac{\partial x_2}{\partial \xi} \\ \frac{\partial x_1}{\partial \eta} & \frac{\partial x_2}{\partial \eta} \end{bmatrix} \qquad J_s = \frac{L_e}{2} \tag{49}
$$

where L_e represents the edge length. In Eq. (46), we multiply the determinant of these jacobians appropriately.

Getting back to Eq. (45), we combine terms with similar variational variables,

$$
\delta \bar{u}^T \left(-[C]\bar{u} + [G]\bar{\mu} + [\hat{F}] + [\hat{T}] \right) + \delta \bar{\mu}^T \left([B]\bar{\mu} + [G]^T \bar{u} - [\hat{\Omega}] \right) = 0 \tag{50}
$$

Since the variational terms δu and $\delta\mu$ are completely arbitrary and independent of each other, terms associated with each variational quantity should be zero. As a result,

$$\begin{aligned} -[C]\bar{u} + [G]\bar{\mu} + [\hat{F}] + [\hat{T}] = 0 \\ [B]\bar{\mu} + [G]^T\bar{u} - [\hat{\Omega}] = 0 \end{aligned} \tag{51}$$

Finally rearranging and writing Eq. (51) in matrix format, we obtain

$$\begin{bmatrix} [C] & -[G] \\ -[G]^T & -[B] \end{bmatrix} \begin{bmatrix} \bar{u} \\ \bar{\mu} \end{bmatrix} = \begin{bmatrix} [\hat{F}] + [\hat{T}] \\ [\hat{\Omega}] \end{bmatrix} \tag{52}$$

This is the final matrix equation analogous to $KU = F$. For an individual element, each term on the left hand side of Eq. (52) is a 8 x 8 matrix. On the right hand side, we expect an 8 x 1 matrix and $[\hat{F}]$ is 8 x 1, but $[\hat{T}]$ and $[\hat{\Omega}]$ are 4 x 1. These should be assembled correctly in the 8 x 1 matrix, based on the surfaces on which the traction and rotations are applied.

Also we see that the applied force traction and rotation boundary conditions are present on the right hand side. These are the so called Neumann boundary conditions. The Dirichlet boundary conditions, which in this formulation are the displacement and moment traction boundary conditions, have to be enforced further at the nodes. There are many ways this can be done. Here it is accomplished by replacing the right hand side with the given value of the boundary condition and then making the corresponding row as zeros and diagonal element as unity in the stiffness matrix. Also, the corresponding column in the stiffness matrix is replaced by zeros to maintain the symmetry and the right hand side is modified accordingly.

Note that in this mixed formulation, the role of rotation and moment-traction boundary condition is reversed from a displacement based method. Generally in finite elements, displacement-like quantities act as Dirichlet boundary conditions and force-like quantities are applied on the right hand side. Instead in this formulation, the moment-traction boundary condition has to be fulfilled essentially on couple traction vectors, while the rotation boundary has to be applied on the right hand side. To elaborate this we consider the problem in Fig. 1. The object is fixed on the left and bottom surfaces and a traction $\hat{t}$ is applied on the tilted surface. There are no applied moment-tractions, hence these are zero everywhere that rotations are not specified. In 2D plane strain analysis, since only ω_3 is non-zero, only the moment-traction $\hat{m}_3$ will contribute in the variational form. This moment-traction from Eqs. (13) and (15) can be written as $\hat{m}_3 = \mu_2 n_1 - \mu_1 n_2$. Since the right surface has a normal component $n_2 = 0$, the couple stress vector component μ_2 should be zero here. Similarly, because the top surface has $n_1 = 0$, we should have $\mu_1 = 0$. For the tilted surface, whose normal is not aligned with x_1 and x_2, we need to transform the stiffness matrix and the right hand side, such that the couple stress components defined in Eq. (37) consist of nodal variables μ_t aligned with the tangential coordinates of the boundary surface. Then we can set these μ_t to zeros. This example shows how we can always satisfy moment-traction boundary conditions on one component of the couple stress vector essentially in 2D.

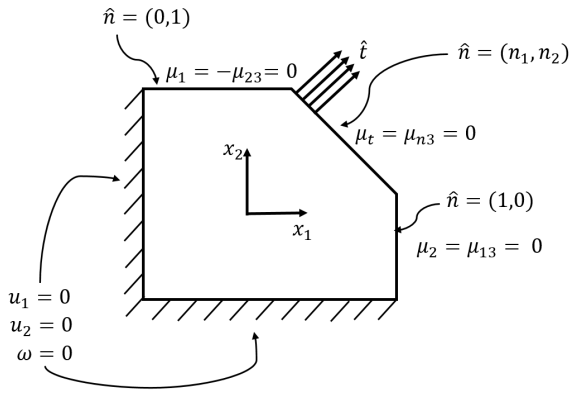

Figure 1: *Schemetic of a model problem to understand boundary conditions*

5. Computational Examples

5.1. Isotropic Material

The finite element formulation presented in the previous section should be validated first before presenting results for anisotropic materials. We analyze isotropic materials to compare with the previous work in this area. For isotropic materials, we have two independent parameters in the stress - strain constitutive matrix C and one independent parameter in the couple stress - curvature constitutive matrix D. Material parameters for examples presented in this subsection are shear modulus $G = 1$ Mbar (Mbar = Megabar = 10^{11} Pascal) and Poisson's ratio $\nu = 0.25$. Therefore, we can write our C and D matrix for 2D planar problems as

$$C = \begin{bmatrix} 3 & 1 & 0 \\ 1 & 3 & 0 \\ 0 & 0 & 1 \end{bmatrix} Mbar \qquad D = 4 \begin{bmatrix} \eta & 0 \\ 0 & \eta \end{bmatrix} Mbar\ m^2 \tag{53}$$

Here η in the D matrix has the dimension of stress times square of length (Mbar m^2), hence we express it as

$$\frac{\eta}{G} = l^2 \tag{54}$$

The l above is defined as the characteristic material length, which is unique for a material but unknown at this point. Therefore, results with varying ratio of characteristic material length with geometric length (l/a) are presented. This basically means that the effect of couple stress theory is studied for different geometric sizes of the structure.

5.1.1. Plate with a Hole

A classic example of a square plate with a hole at the center is taken. Since this plate is symmetric about a horizontal and vertical line passing through the center, its quarter part is taken for analysis as shown in Fig. 2. The ratio $H/a = 2$ for this analysis. The quarter plate is on roller joints on the left and bottom surface, which allows only sliding. A constant horizontal traction of $t_0 = 0.5$ kbar (kbar = kilobar = 10^8 Pascal) is applied on the right surface. To maintain the symmetry, we also set the rotation ω on the left and the bottom surfaces equal to zero. This essentially means that in our formulation we set couple stress μ_t on the top, right and circular surface equal to zero (details described in Fig. 1). The results for a finite element mesh of 1924 elements are tabulated in Table 1 and compared with those presented in Hadjesfandiari and Dargush (2012).

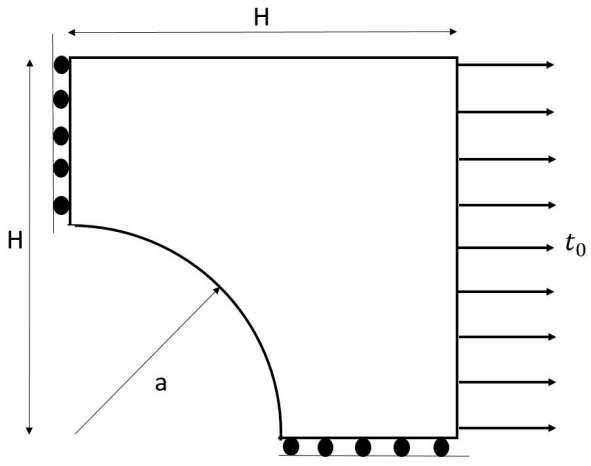

Figure 2: Schemetic of a quarter of a plate with a hole

Table 1: Comparison of isotropic plate with a hole with BEM solutions

	l/a	**BEM 160**	**FEM 1924**
$\mathbf{U_{CL}}$ $\left(a \text{ x } 10^{-3}\ m\right)$	10^{-4}	1.4634	1.4620
	0.25	0.9387	0.9384
	0.5	0.7051	0.7049
	1	0.6038	0.6037
$\mathbf{U_{TC}}$ $\left(a \text{ x } 10^{-3}\ m\right)$	10^{-4}	0.1464	0.1470
	0.25	0.3557	0.3559
	0.5	0.4617	0.4618
	1	0.5102	0.5102
SCF	10^{-4}	3.2018	3.1989
	0.25	2.0058	2.0060
	0.5	1.4998	1.4995
	1	1.2866	1.2872

Here U_{CL} is the horizontal displacement of the bottom right corner and U_{TC} is the horizontal displacement of the top right corner, while SCF is the stress concentration factor. It is seen that the deflections decrease with increasing l/a ratio. This shows that the material becomes stiffer as we approach sizes near the material length scale l. Also the stress concentration factor approaches to unity as the geometry approaches the material length scale. Stress contours of σ_{11} in Fig. 3 also show the reduced stress concentration factor. Results are also verified with those presented in Hadjesfandiari and Dargush (2012), which confirms that the implementation is correct.

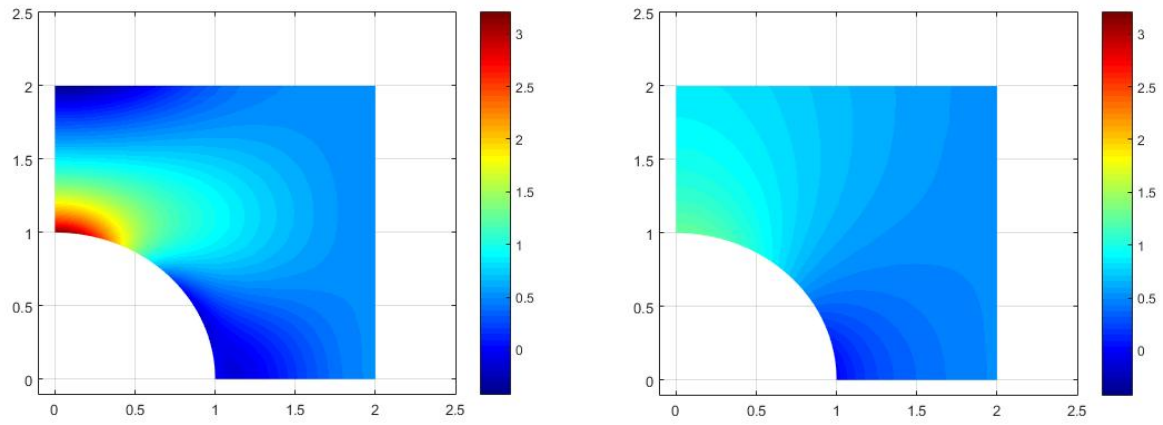

(a) $l/a = 10^{-4}$ (b) $l/a = 1$

Figure 3: σ_{11} contour on isotropic plate with a hole

5.1.2. Cantilever beam

We now take the example of a plane strain cantilever beam fixed at the left end as shown in Fig. 4. The length (L) to height (h) ratio of this beam is 20. A traction of $t_0 = 0.01$ kbar is applied on the right surface, as illustrated. Displacements and rotations are both assumed to be zero at the left surface.

Figure 4: Schemetic of a cantilever beam

First we carry out a convergence study. The cantilever beam above is meshed in such a way that the length is divided 20 times more than the height to get an element aspect ratio of 1. The number of mesh elements is increased and the total deformation energy for four l/a ratios is plotted against the number of elements in Fig. 5. We see that total deformation energy shows nice convergence at all four l/a ratios. However, notice that the convergence is slowest for the smallest l/a ratio. For this case, l is small compared to a typical element size, which causes some inaccuracy.

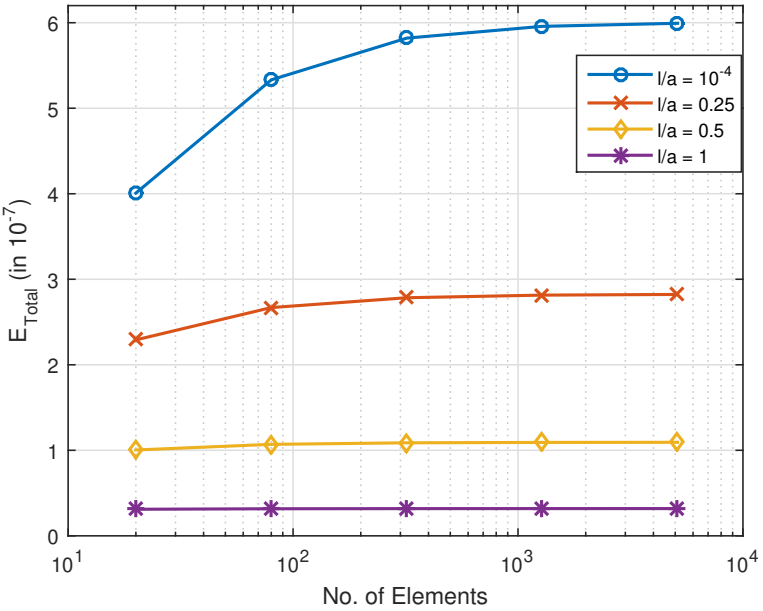

Figure 5: Convergence study of the total energy

A study on condition number of the stiffness matrix for this formulation was also carried out. The condition number for l/a between 10^{-2} to 10^2 is less than 10^8. This covers the couple stress active region where $l/a > 10^2$ represents very small scale for which continuity of the material becomes questionable, while $l/a < 10^{-2}$ represents the classical regime for which couple stresses are negligible. The condition number can become huge for these extreme length scales. To reduce this condition number, one can do preconditioning of the matrix. For example, a Jacobi preconditioner can be used to bring the condition number down significantly to the order of 10^3.

Next, the effect of l/a ratio on the stiffness of the cantilever beam is studied. We have taken two cases here, the first one in which the cantilever has zero rotation on the fixed end and the second one in which the rotations are free on the fixed end. From Euler Bernoulli beam bending theory, the stiffness of the beam is $3EI/L^3$. Stiffness K from the current finite element formulation is calculated by taking ratio of load with deflection at the right end. Then the quantity $KL^3/3EI$ can be defined as non-dimensional stiffness (NDS). This non-dimensional stiffness is plotted with varying l/a ratio in Fig. 6, which reproduces the behavior found in Darrall et al. (2014). It can be seen that for $l/a < 0.1$, the non-dimensional stiffness is close to unity and hence represents the classical elasticity region. Next in the region between $l/a = 0.1$ to $l/a = 100$ labeled as couple stress elasticity, the non-dimensional stiffness increases steeply and hence shows a high size dependency. The last region $l/a > 100$, non-dimensional stiffness reaches the value of nearly 2600 and saturates. This region is labeled as couple stress saturation Darrall et al. (2014). Similar behavior is displayed in Fig. 7 for the case with zero couple traction(or free macrorotations) at the fixed end, except that the NDS saturates at a much lower level of approximately 31. Stress contours of σ_{11} for classical elasticity and couple stress saturated regions for zero and free macrorotations at fixed end are shown in Fig. 8. These contours show that in the classical elasticity region, the normal force stress σ_{11} is varying and has opposite sign on top and bottom of the center-line of the beam, which creates the bending moment. In the couple stress saturation state, the force stress σ_{11} becomes small and nearly constant over the height. This creates a pure shear mode and locks up beam bending, making it more stiff. Instead couple stress μ_2 becomes active and supports the bending moment.

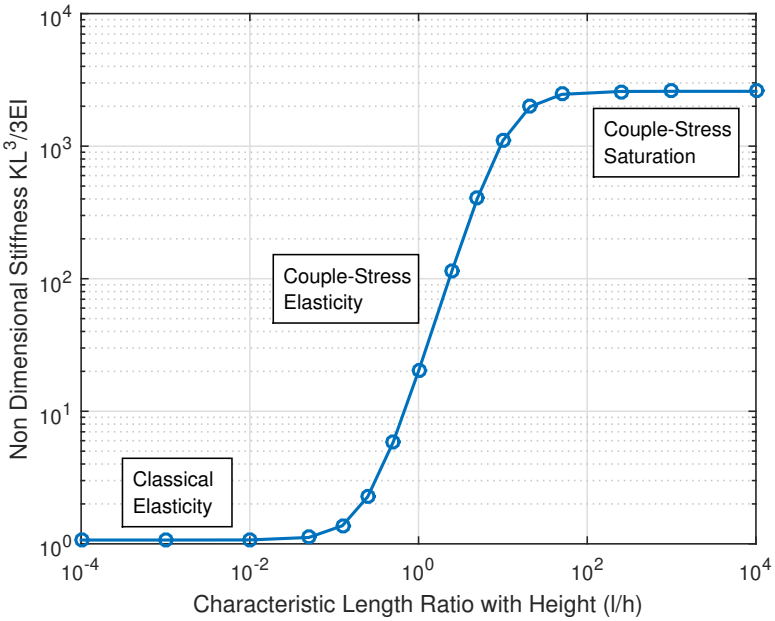

Figure 6: Non-dimensional stiffness vs l/h for $\omega = 0$ on fixed end

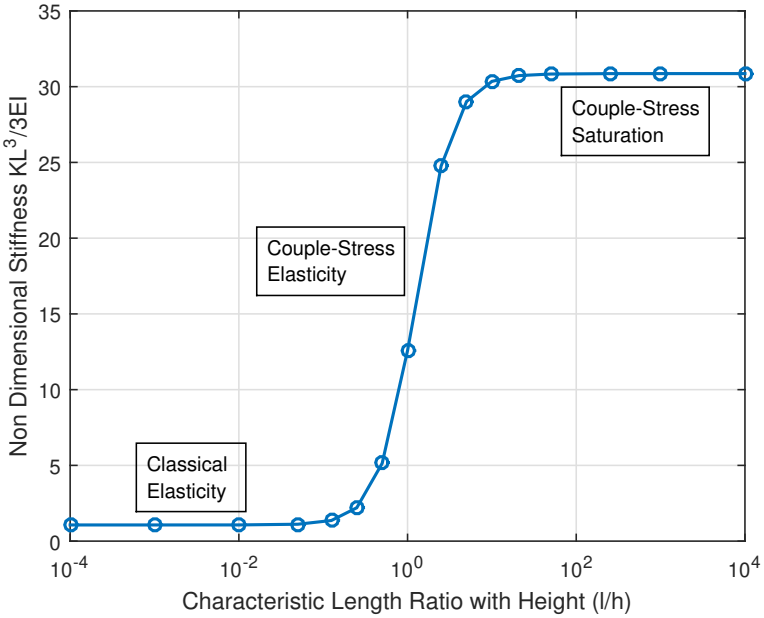

Figure 7: Non-dimensional stiffness vs l/h for free ω on fixed end

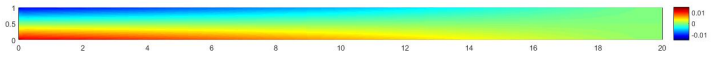

(a) Classical Elasticity (NDS ≈ 1)

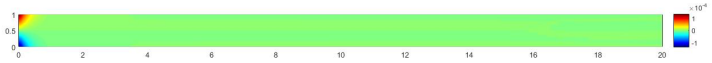

(b) Couple Stress Saturated (NDS ≈ 2592) for $\omega = 0$ on fixed end

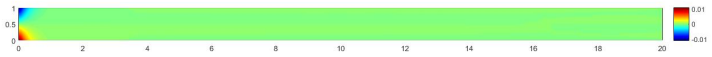

(c) Couple Stress Saturated (NDS ≈ 31) for free ω on fixed end

Figure 8: σ_{11} contour of isotropic cantilever beam

5.2. Anisotropic Materials

In the following subsections, responses for different anisotropic symmetry classes are examined under the same two basic problems studied for the isotropic case in Sections 5.1.1 and 5.1.2. Thus we consider (1) the square plate with a central circular hole with H/a = 2 under uniaxial loading for t_0 around 0.5 kbar and (2) cantilever beam bending with $L/h = 20$, fully fixed on the left end and loaded by uniform shear traction t_0 around 0.01 kbar on the right edge. We will only take the case of $\omega = 0$ on the fixed end for this cantilever beam example.

5.3. Cubic Single Crystal

Next, the analysis is presented for copper single crystal, which is a cubic crystal of class $m3m$. This material is centrosymmetric and has three independent parameters in the stress - strain constitutive matrix C and one independent parameter in the couple stress - curvature constitutive matrix D Nye (1985). Constitutive C and D matrices for 2D planar problems are written as:

$$C = \begin{bmatrix} 1.7637 & 1.2920 & 0 \\ 1.2920 & 1.7637 & 0 \\ 0 & 0 & 0.7519 \end{bmatrix} Mbar \qquad D = 4 \begin{bmatrix} \eta & 0 \\ 0 & \eta \end{bmatrix} Mbar\ m^2 \tag{55}$$

Values of material parameters in the C matrix are taken from Nye (1985) and those in D are unknown. In anisotropic materials, the number of independent parameters are more and hence these are generally represented in terms of constitutive relations coefficient (e.g. C_{11},C_{12}, etc.) instead of Young's modulus, shear modulus or Poisson's ratio. Therefore η in the couple stress - curvature constitutive matrix D is defined as,

$$\eta / C_{66} = l^2 \tag{56}$$

As explained for isotropic material, l is the characteristic material length scale and results will be presented versus a varying l/a ratio.

5.3.1. Plate with a hole

Again the example of a plate with a hole is presented as in Fig. 2 of the previous subsection. For single crystal materials, it is very important to know the axis orientation of the crystal with respect to the geometry. In this current example, the axis x_1 of the crystal is assumed to align with the horizontal lines of the plate. A traction of $t_0 = 0.2$ kbar is applied on the right surface. Results with varying l/a ratio are tabulated in Table 2. Comparing Tables 1 and 2, we see that the values of SCF in copper single crystal are less than those for an isotropic material for all l/a ratios. Also stress contours of σ_{11} are shown for $l/a = 10^{-4}$ and $l/a = 1$ in Fig. 9, which are a little different from those of an isotropic material. Notice that in Fig. 9b for copper single crystals, the contours are much more vertical above the hole, leading to a reduced SCF for all of the material length scales to maintain quarter symmetry.

Table 2: Results of copper (Cu) single crystal with varying l/a ratios

l/a	U_{CL} $\left(a \text{ x } 10^{-3}\ m\right)$	U_{TC} $\left(a \text{ x } 10^{-3}\ m\right)$	SCF
10^{-4}	1.5465	0.2057	2.6513
0.25	0.9190	0.5545	1.4988
0.5	0.7581	0.6411	1.2038
1	0.7037	0.6699	1.1042

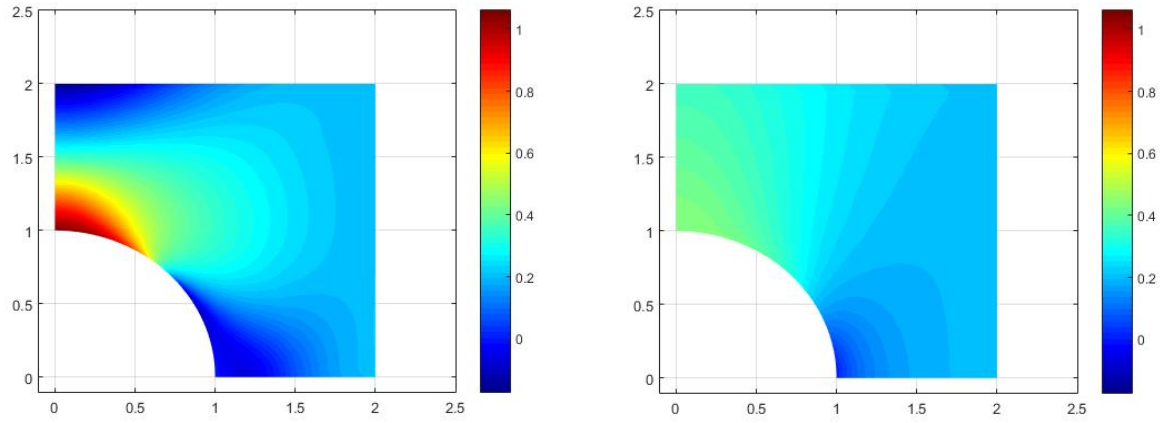

(a) $l/a = 10^{-4}$ (b) $l/a = 1$

Figure 9: σ_{11} contour on copper (Cu) single crystal plate with a hole

5.3.2. Cantilever beam

We again take the cantilever beam, as shown in Fig. 4. Non-dimensional stiffness (NDS) is plotted with varying l/a ratios in Fig. 10. We see that NDS of copper single crystal cantilever reaches a value of nearly 7250 which is significantly larger than that of an isotropic material (2600). Stress contours σ_{11} for classical elasticity and couple stress saturated regions are shown in Fig. 11. The contours show the similar trend as in the isotropic material of Section 5.1. The varying normal stress σ_{11} becomes nearly constant in the couple stress saturated region due to full activation of couple stress, hence making the beam dramatically stiffer.

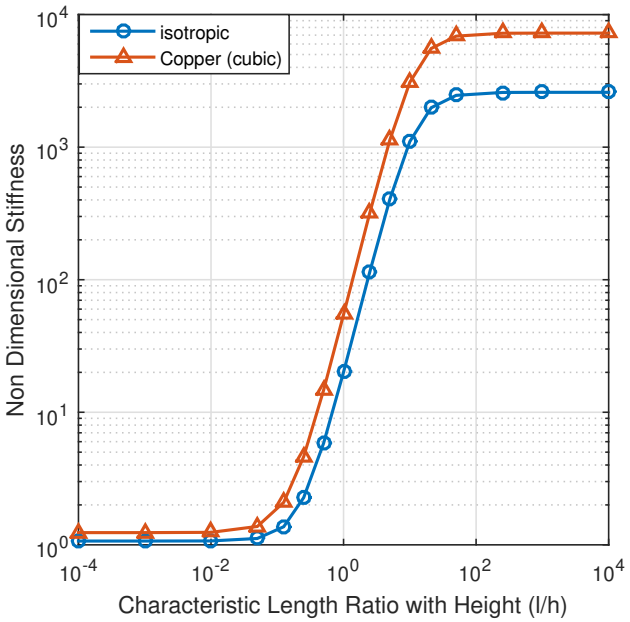

Figure 10: Non-dimensional stiffness vs l/a for copper (Cu) single crystal

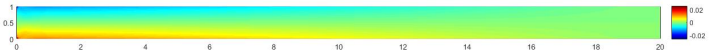

(a) Classical Elasticity (NDS ≈ 1)

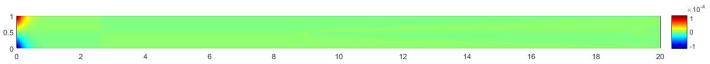

(b) Couple Stress Saturated (NDS ≈ 7250)

Figure 11: σ_{11} contour of copper (Cu) single crystal cantilever beam

5.3.3. Crystals not aligned with geometric axis

In Sections 5.3.1 and 5.3.2, we analyzed problems in which the copper crystal axis was aligned with the geometric axis. In this section, we will take the same two problems, but instead, will solve for copper crystals aligned 45 degrees to the geometric x_1 axis. We will call this Copper Single Crystal 45°. Since we will be solving the problem in the same geometric axis (x_1x_2), we need to transform the constitutive matrices appropriately from material coordinate system to the chosen geometric coordinate system. Thus,

$$C = \begin{bmatrix} 2.2798 & 0.7759 & 0 \\ 0.7759 & 2.2798 & 0 \\ 0 & 0 & 0.2359 \end{bmatrix} Mbar \qquad D = 4 \begin{bmatrix} \eta & 0 \\ 0 & \eta \end{bmatrix} Mbar\ m^2 \tag{57}$$

In Eq. (57), we see that anisotropy changes the force stress-strain constitutive matrix C but not the couple stress-curvature constitutive matrix D, since D is isotropic. Now, we will use the above constitutive matrices to compute results for the same problems of the plate with a hole and the cantilever beam defined in Sections 5.3.1 and 5.3.2.

Table 3: Results of copper (Cu) single crystal 45° for varying l/a ratios

l/a	$\mathbf{U_{CL}}$ $\left(a \text{ x } 10^{-3}\ m\right)$	$\mathbf{U_{TC}}$ $\left(a \text{ x } 10^{-3}\ m\right)$	**SCF**
10^{-4}	1.0966	0.0748	4.2630
0.25	0.5890	0.1824	2.2875
0.5	0.4350	0.2344	1.7526
1	0.3734	0.2595	1.5427

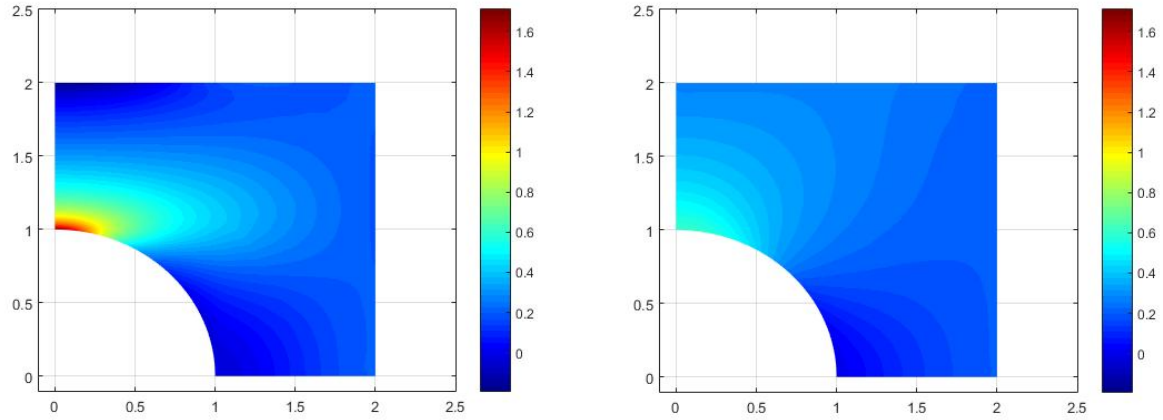

(a) $l/a = 10^{-4}$ (b) $l/a = 1$

Figure 12: σ_{11} contour on copper (Cu) single crystal 45° plate with a hole

We see that the SCF for the plate with a hole in Table 3 is quite a bit larger than Table 2, basically showing that the SCF are higher when the material coordinate axes of Copper Single Crystal are aligned at 45^o with the geometric axis. These SCF are also higher than that of isotropic material in Table 1, which is also suggested by more horizontal stress contours in Fig 12, when compared to Fig 3. Nevertheless, as we approach the material length scale, the SCF drops from 4.26 to 1.54, showing the energy is being stored as curvature energy.

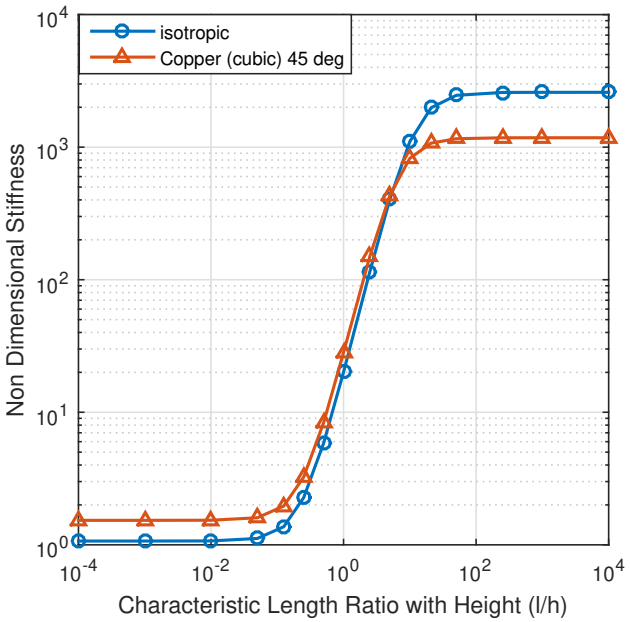

Figure 13: Non-dimensional stiffness vs l/a for copper (Cu) single crystal 45°

In Fig 13, we can see that the non-dimensional stiffness for Copper Single Crystal 45^o cantilevers is equal to one for low l/a values and saturates to 1178 for very high l/a values. This NDS saturation value is less than that of the isotropic material and is significantly less than that of copper single crystal aligned with the geometric axis as shown in Fig 10. Clearly, for copper single crystal under couple stress theory, the response is quite sensitive to orientation.

5.4. Hexagonal Single Crystal

Next we take zinc (Zn) single crystal, which is a hexagonal crystal of class $6/mmm$. This class is centrosymmetric and has five independent parameters in the stress strain constitutive matrix C and two independent parameters in the couple stress - curvature constitutive matrix D Nye (1985). For 2D planar problems, this reduces to two independent parameters in C and one independent parameter in D. Therefore these constitutive matrices can be written as:

$$C = \begin{bmatrix} 1.6355 & 0.2656 & 0 \\ 0.2656 & 1.6355 & 0 \\ 0 & 0 & 0.6849 \end{bmatrix} Mbar \qquad D = 4 \begin{bmatrix} \eta & 0 \\ 0 & \eta \end{bmatrix} Mbar\ m^2 \tag{58}$$

The material parameters in the C matrix are taken from Nye (1985). Material parameter η can be defined in terms of characteristic length scale l as defined in Eq. (55). Results of computational examples will be presented with varying l/a ratio.

5.4.1. Plate with a hole

We take the example of a plate with a hole shown in Fig. 2. Again in our analysis, axis x_1 of the crystal is assumed to align with the horizontal and traction of $t_0 = 0.3$ kbar is applied on the right surface. The results for deflections and stress concentration factor with varying l/a ratio are shown in Table 4. We see that the SCF is very close to those for isotropic material in Table 1. This is because in 2D plane strain and the choice of axis selected for the current example, the constitutive matrix C for hexagonal crystal has the plane of isotropy with an effective Poisson's ratio of 0.14. Stress contours for σ_{11} for $l/a = 10^{-4}$ and $l/a = 1$ are shown in Fig. 14, which are similar to those of isotropic materials.

Table 4: Results of zinc (Zn) single crystal with varying l/a ratios

l/a	$\mathbf{U_{CL}}$ $\left(a \text{ x } 10^{-3}\ m\right)$	$\mathbf{U_{TC}}$ $\left(a \text{ x } 10^{-3}\ m\right)$	**SCF**
10^{-4}	1.4690	0.1478	3.1941
0.25	0.9090	0.3707	1.9226
0.5	0.6850	0.4710	1.4421
1	0.5926	0.5141	1.2481

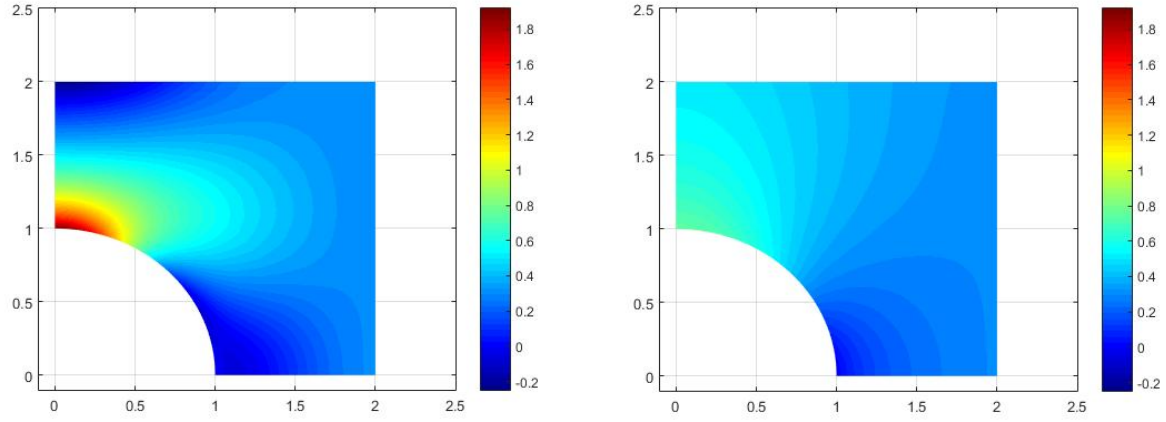

(a) $l/a = 10^{-4}$ (b) $l/a = 1$

Figure 14: σ_{11} contour on zinc (Zn) single crystal plate with a hole

5.4.2. Cantilever Beam

The cantilever beam shown in Fig. 4 of zinc single crystal whose x_1 axis aligns with the horizontal is taken for the analysis. Non-dimensional stiffness is plotted with varying l/a ratios and compared to isotropic material in Fig. 15. We see that NDS of the zinc single crystal beam rises from unity to nearly 3700 and is somewhat higher than NDS for the isotropic material. Stress contours σ_{11} for classical elasticity and couple stress saturated regions are shown in Fig. 16 and are similar to those of isotropic materials, as expected due to the isotropy of the $x_1 - x_2$ plane.

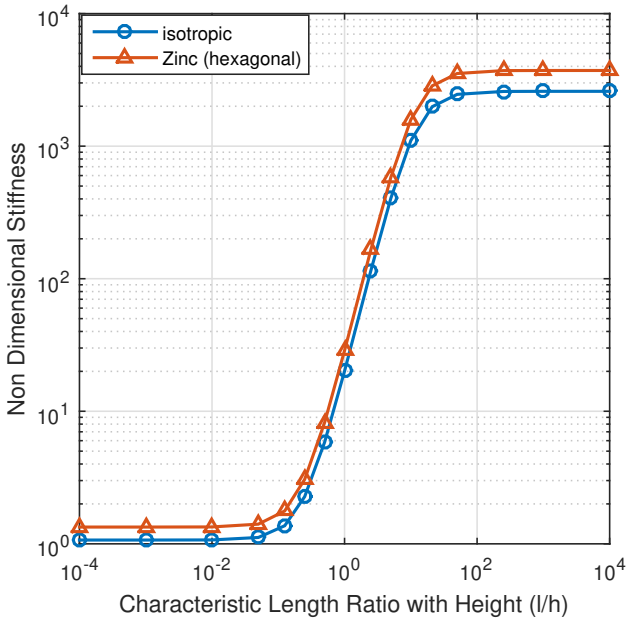

Figure 15: Non-dimensional stiffness vs l/a for zinc (Zn) single crystal

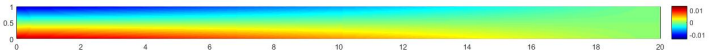

(a) Classical Elasticity (NDS ≈ 1)

(b) Couple Stress Saturated (NDS ≈ 3724)

Figure 16: σ_{11} contour of zinc (Zn) single crystal cantilever beam

5.5. Trigonal Single Crystal

Next, examples of trigonal single crystal are presented. We take antimony (Sb) single crystal, which is of class $\bar{3}m$ and has a center of symmetry. This class of crystal has six independent parameters in the stress - strain constitutive matrix C and two independent parameters in the couple stress - curvature constitutive matrix D Nye (1985). For 2D planar problems, this reduces to two independent parameters in C and one independent parameter in D. Hence, the C and D matrices can be written as below:

$$C = \begin{bmatrix} 0.7916 & 0.2474 & 0 \\ 0.2474 & 0.7916 & 0 \\ 0 & 0 & 0.2721 \end{bmatrix} Mbar \qquad D = 4 \begin{bmatrix} \eta & 0 \\ 0 & \eta \end{bmatrix} Mbar\ m^2 \tag{59}$$

The material parameters in C are taken from Simmons et al. (1971) for antimony (code 62836). The parameter η is the same as defined in Eq. (55) and can be expressed in terms of characteristic material length scale l.

5.5.1. Plate with a hole

The plate with a hole in Fig. 2 is analyzed with the axis x_1 of the crystal aligned with the horizontal. A traction of 0.14 kbar is applied on the right surface. Results with varying l/a ratio are tabulated in Table 5. Again we see that these values of SCF are very close to those presented for the isotropic material in Table 1. This is because of the fact that the trigonal crystal has isotropy in x_1-x_2 plane and we have selected those two axes in our 2D plane strain problems. The stress contours of σ_{11} are also plotted for $l/a = 10^{-4}$ and $l/a = 1$ as displayed in Fig. 17, which shows a similar trend of reduced SCF as that in the isotropic materials.

Table 5: Results of antimony (Sb) single crystal with varying l/a ratios

l/a	$\mathbf{U_{CL}}$ $\left(a \text{ x } 10^{-3}\ m\right)$	$\mathbf{U_{TC}}$ $\left(a \text{ x } 10^{-3}\ m\right)$	**SCF**
10^{-4}	1.5283	0.1537	3.2006
0.25	0.9768	0.3736	1.9967
0.5	0.7340	0.4836	1.4927
1	0.6293	0.5335	1.2826

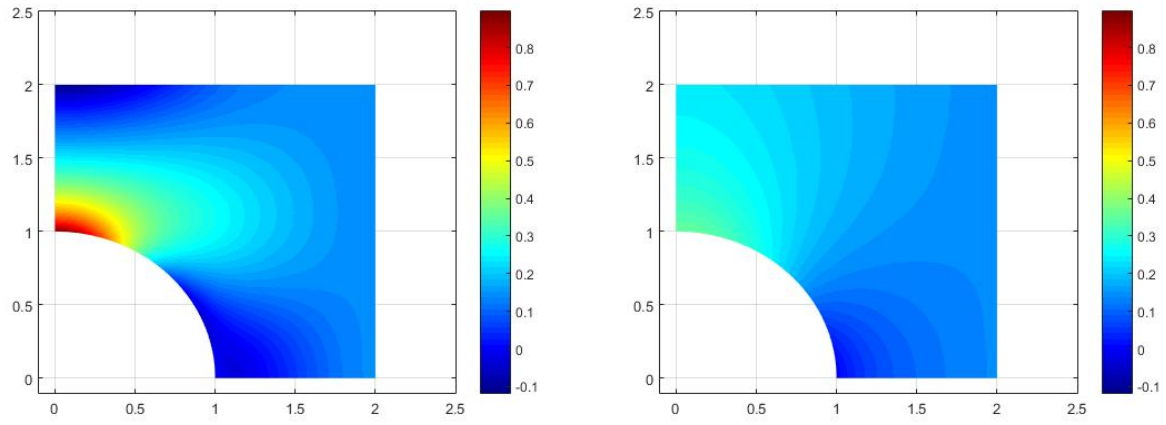

(a) $l/a = 10^{-4}$ (b) $l/a = 1$

Figure 17: σ_{11} contour on antimony (Sb) single crystal plate with a hole

5.5.2. Cantilever Beam

We take an antimony single crystal cantilever beam shown in Fig. 4. Non-dimensional stiffness is plotted versus increasing l/h ratio in Fig. 18. These stiffness values are very close to those obtained for the isotropic material. Stress contour σ_{11} for classical elasticity and couple stress saturated regions are shown in Fig. 19 and are similar to those obtained for the isotropic material with $E = 0.67$ MBar and $\nu = 0.24$.

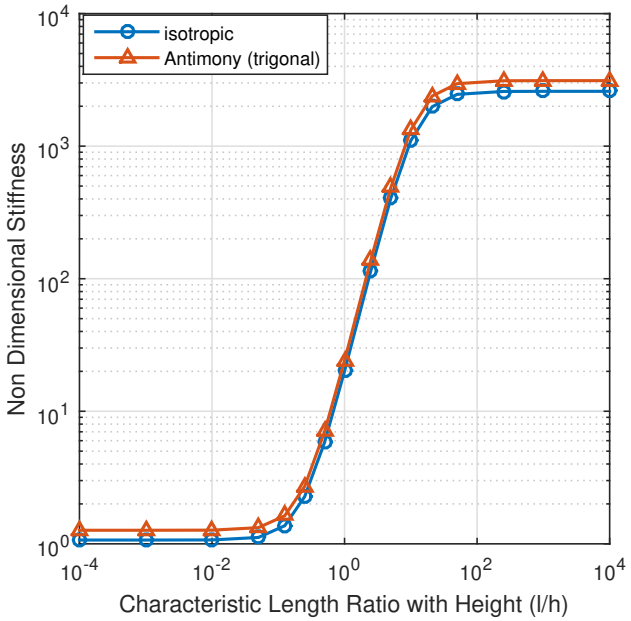

Figure 18: Non-dimensional stiffness vs l/a for antimony (Sb) single crystal

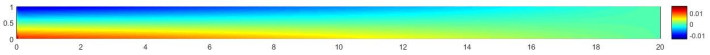

(a) Classical Elasticity (NDS ≈ 1)

(b) Couple Stress Saturated (NDS ≈ 3121)

Figure 19: σ_{11} contour of antimony (Sb) single crystal cantilever beam

5.6. Tetragonal Single Crystal

Next for our analysis we take tin (Sn) single crystals, which has a tetragonal crystal structure of class $4/mmm$ that is centrosymmetric. It has six independent material parameters in the stress - strain constitutive matrix C and two independent parameters in the couple stress - curvature constitutive matrix D Nye (1985). For two dimensions, this reduces to three parameters in C and one parameter in D. Therefore, these matrices can be written as:

$$C = \begin{bmatrix} 0.8391 & 0.4870 & 0 \\ 0.4870 & 0.8391 & 0 \\ 0 & 0 & 0.0741 \end{bmatrix} Mbar \qquad D = 4 \begin{bmatrix} \eta & 0 \\ 0 & \eta \end{bmatrix} Mbar\ m^2 \tag{60}$$

The values of parameters in C are taken from Nye (1985). The material parameter η in D matrix can be specified in terms of a characteristic length scale as defined in Eq. (55).

5.6.1. Plate with a hole

The plate with a hole described in Fig. 2 is taken for analysis of tin single crystal. A traction of 0.08 kbar is applied on the right surface. Results with varying l/a ratio are tabulated in Table 6. We see that the SCF for tin at all length scales is significantly higher than for the isotropic material. Stress contours of σ_{11} are also plotted for $l/a = 10^{-4}$ and $l/a = 1$, as shown in Fig. 20, which has a similar trend of stress reduction as the isotropic material, but the contours are slightly different.

Table 6: Results of tin (Sn) single crystal with varying l/a ratios

l/a	$\mathbf{U_{CL}}$ $\left(a \text{ x } 10^{-3}\ m\right)$	$\mathbf{U_{TC}}$ $\left(a \text{ x } 10^{-3}\ m\right)$	**SCF**
10^{-4}	1.4713	0.1086	4.0718
0.25	1.0514	0.2018	2.8237
0.5	0.7647	0.2901	2.0957
1	0.5900	0.3580	1.6606

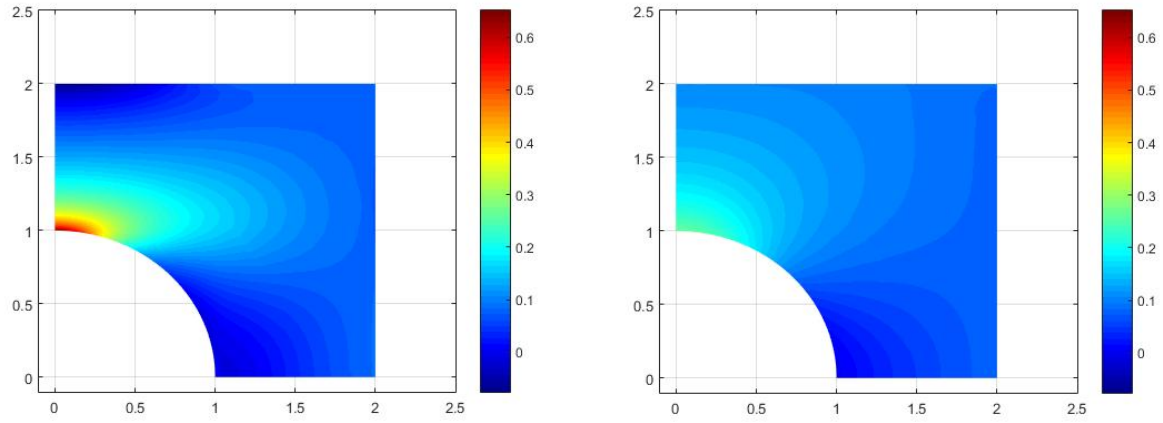

(a) $l/a = 10^{-4}$ (b) $l/a = 1$

Figure 20: σ_{11} contour on tin (Sn) single crystal plate with a hole

5.6.2. Cantilever Beam

We take the tin (Sn) single crystal cantilever beam, as shown in Fig. 4. The axis x_1 of the crystal points along the length of the beam. Non-dimensional stiffness (NDS) is plotted versus varying l/a ratio in Fig. 21. It turns out that at couple stress saturation, tin has a low NDS of nearly 900, as compared to that of the isotropic material (2600). Stress contour σ_{11} for classical elasticity and couple stress saturated regions are shown in Fig. 22 and reveals that at couple stress saturation, as with an isotropic material, the normal stress are too small to produce any bending moment and hence the beam becomes stiffer.

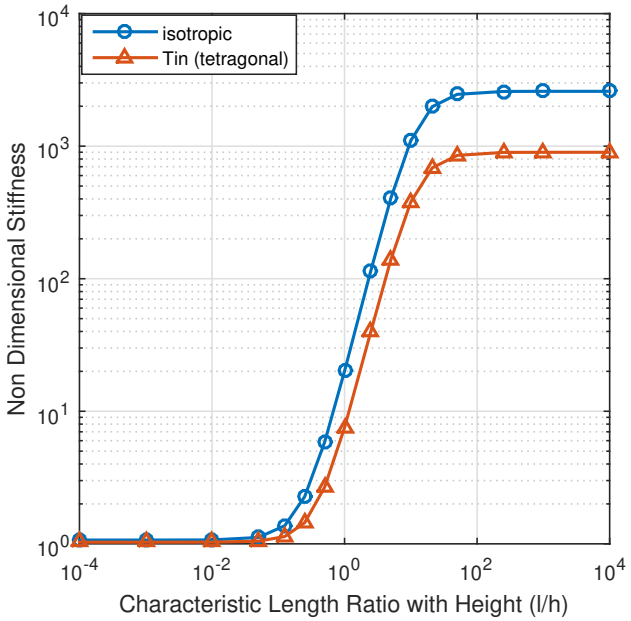

Figure 21: Non-dimensional stiffness vs l/a for tin (Sn) single crystal

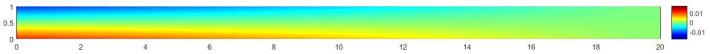

(a) Classical Elasticity (NDS ≈ 1)

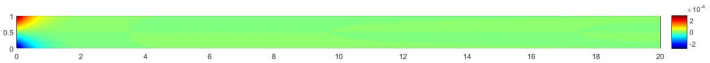

(b) Couple Stress Saturated (NDS ≈ 899)

Figure 22: σ_{11} contour of tin (Sn) single crystal cantilever beam

5.7. Orthorhombic Single Crystal

Lastly, we take aragonite single crystals for our final material. Aragonite has an orthorhombic crystal structure of class *mmm* and is centrosymmetric. It has nine independent material parameters in the stress - strain constitutive matrix C and three more independent parameters in the couple stress - curvature constitutive matrix D Nye (1985). We take the problems where the axes x_1 and x_2 of the crystal lie in our two dimensional plane. This assumption reduces the number of parameters to four in C and two in the D matrix, which can be written as shown below:

$$C = \begin{bmatrix} 1.5958 & 0.3663 & 0 \\ 0.3663 & 0.8697 & 0 \\ 0 & 0 & 0.4274 \end{bmatrix} Mbar \qquad D = 4 \begin{bmatrix} \eta_1 & 0 \\ 0 & \eta_2 \end{bmatrix} Mbar\ m^2 \tag{61}$$

The values of parameters in the C matrix are taken from Simmons et al. (1971). This is the first and only example taken which has two different parameters in the couple stress - curvature constitutive matrix. These are defined as follows:

$$\frac{\eta_1}{C_{66}} = l_1^2 \qquad \frac{\eta_2}{C_{66}} = l_2^2 \tag{62}$$

We see that this material has two characteristic length scales in D. Results in the following subsections will be presented with varying l_1/a and l_2/l_1 ratios.

5.7.1. Plate with a hole

As described in previous subsections, the example of a square plate with a hole is taken with the axis x_1 of the crystal aligned with the horizontal. A traction of 0.23 kbar is applied on the right surface. Results with varying l_1/a and l_2/l_1 ratio are tabulated in Table 7 and are plotted in Fig. 23. We see that for an l_2/l_1 ratio of 0.1 and 1, the SCF values of aragonite are higher than those of the isotropic material for $l/a < 1$. For $l_2/l_1 = 10$, the SCF is higher only for $l/a < 0.1$ and then drops a certain amount below that of the isotropic value and remains constant. The stress contours of σ_{11} are also plotted for $l/a = 10^{-4}$ and $l/a = 1$ for three different l_2/l_1 ratio as shown in Fig. 24. These contours are similar to those of the isotropic material in terms of reduction of stress concentration factor but have a slight difference in contours corresponding to $l_2/l_1 = 0.1$ and $l/a = 1$ in Fig. 24b.

Table 7: Results of aragonite single crystal with varying l_1/a and l_2/l_1 ratios

l_2/l_1	l_1/a	U_{CL} $\left(a \text{ x } 10^{-3}\ m\right)$	U_{TC} $\left(a \text{ x } 10^{-3}\ m\right)$	SCF
0.1	10^{-4}	1.5096	0.0269	3.7277
	0.25	1.0493	0.1894	2.8307
	0.5	0.7669	0.3340	2.2258
	1	0.6004	0.4261	1.8112
1	10^{-4}	1.5096	0.0269	3.7277
	0.25	0.9017	0.2604	2.2365
	0.5	0.6450	0.3768	1.6146
	1	0.5363	0.4297	1.3535
10	10^{-4}	1.5096	0.0269	3.7277
	0.25	0.5806	0.4481	1.2877
	0.5	0.5204	0.4512	1.2532
	1	0.4999	0.4517	1.2509

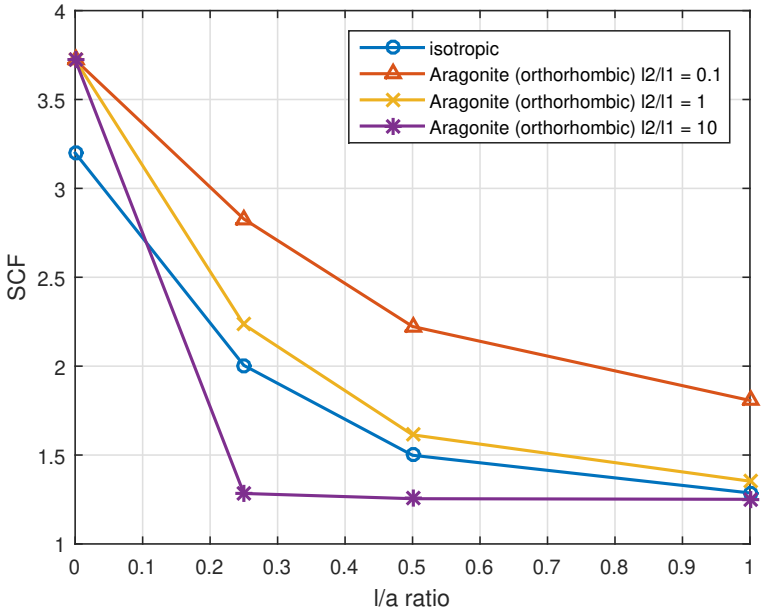

Figure 23: SCF vs l/a for aragonite single crystal

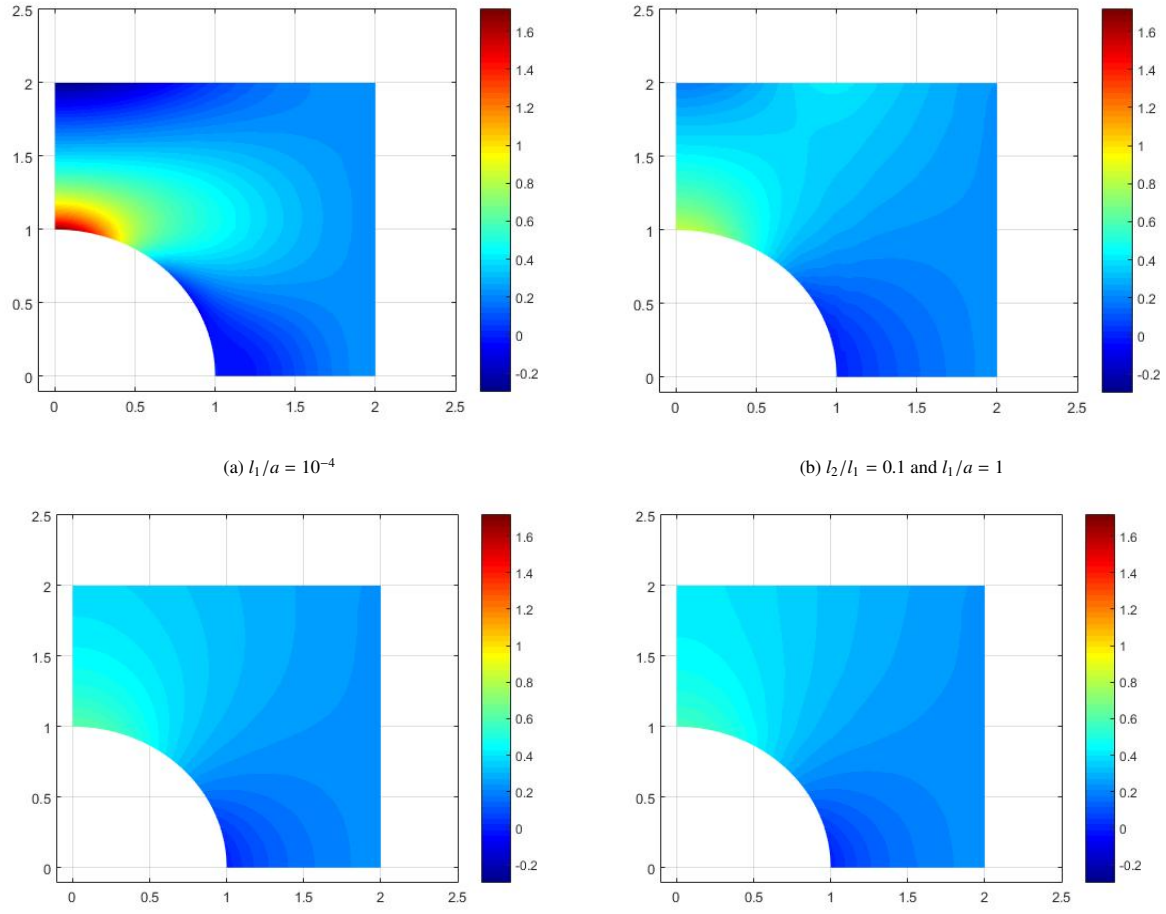

(a) $l_1/a = 10^{-4}$

(b) $l_2/l_1 = 0.1$ and $l_1/a = 1$

(c) $l_2/l_1 = 1$ and $l_1/a = 1$

(d) $l_2/l_1 = 10$ and $l_1/a = 1$

Figure 24: σ_{11} contour on aragonite single crystal plate with a hole

5.7.2. Cantilever Beam

Finally, we examine an aragonite single crystal cantilever beam shown in Fig. 4. Non-dimensional stiffness (NDS) is plotted with increasing l/a ratio in Fig. 25. It is seen that the ratio of l_2/l_1 determines if the NDS starts increasing at lower or higher values of the l_1/a ratio. In any case, the NDS at couple stress saturation reaches the same value of nearly 1980, which is somewhat lesser than for the isotropic material (2600). Stress contours σ_{11} for classical elasticity and couple stress saturated regions are shown in Fig. 25. The contours show similar reduction of normal stress as that of the isotropic material due to activation of couple stresses resulting in stiffening of the beam.

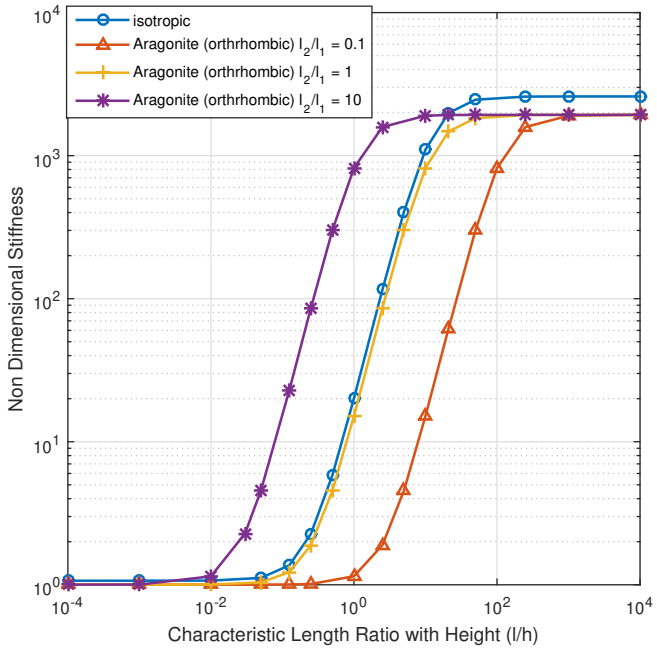

Figure 25: Non-dimensional stiffness vs l/a for Aragonite single crystal

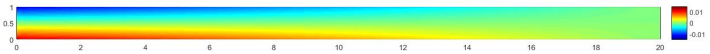

(a) Classical Elasticity (NDS ≈ 1)

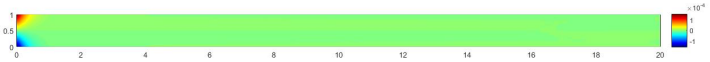

(b) Couple Stress Saturated (NDS ≈ 1982)

Figure 26: σ_{11} contour of aragonite single crystal cantilever beam

6. Conclusion

Consistent couple stress theory Hadjesfandiari and Dargush (2011) is a promising theory, which can characterize the behaviour of materials at all length scales for which a continuum representation is appropriate. It is well known that numerical methods are of great aid in solving complicated problems in elasticity. Hence a novel mixed finite element method is developed in this paper based on consistent couple stress theory. This mixed finite element method is C^0 continuous and avoids the challenges in maintaining C^1 continuity, which would be required if a fully displacement based variational formulation of this theory was implemented. Unlike previous approaches, the present method

utilizes two polar vector variables, namely, the displacement and couple stress vectors, both of which require only C^0 continuity. As an effect, the roles of rotation and moment traction boundary conditions are reversed with the former serving as the natural condition, while the latter becomes an essential condition.

In this paper, anisotropic materials are analyzed using this formulation. There are two main classes of anisotropic material, namely, centrosymmetric and non-centrosymmetric. Only centrosynmmetric classes are studied and presented in the current work. It is shown in Section 5.1 that the solutions match well with the BEM solutions in Hadjesfandiari and Dargush (2012) for the isotropic case and the solutions converge well with the mesh refinement. Computational examples of cubic, hexagonal, trigonal, tetragonal single crystal structures have been presented to show the effects of couple stresses on anisotropic materials. The summary of Stress Concentration Factor (SCF) and Non-Dimensional Stiffness (NDS) for different materials is tabulated in Table 8. In all the examples, couple stress theory shows an effect of stiffening for geometric sizes near and below the material characteristic length scales. Note that l/a for aragonite in table corresponds to l_1/a.

For the plate with a circular hole, based on U_{CL} and U_{TC}, the stiffnesses increase by a factor of two or three as l/r increases into the couple stress saturated regime. This is caused by suppression of the flexural component of the deformation. However, for the cantilever beam example, where bending dominates, the stiffnesses increase by several orders of magnitude with couple stress saturation.

Regarding specific material response, single crystal copper with principal axis aligned with the coordinate axes shows much lower SCF and significantly increased NDS compared to the isotropic material with $\nu = 0.25$. On the other hand, tin exhibits higher SCF and a relative reduction in stiffness as measured by NDS values. However, orientation of the crystal lattice relative to the coordinate axes can have a dramatic influence on both the SCF and NDS values, especially for a highly anisotropic material, such as copper.

Table 8: Summary of SCF in plate with a hole and NDS for cantilever beam for different materials

Material	**Crystal Structure**	**Class**	l/a	**SCF**	**NDS**
Isotropic	Isotropic	Isotropic	10^{-4}	3.20	1
			1	1.29	20.1
Copper	Cubic	$m3m$	10^{-4}	2.65	1
			1	1.10	54.6
Copper 45^o	Cubic	$m3m$	10^{-4}	4.26	1
			1	1.54	28.3
Zinc	Hexagonal	$6/mmm$	10^{-4}	3.19	1
			1	1.25	28.7
Antimony	Trigonal	$\bar{3}m$	10^{-4}	3.20	1
			1	1.28	24.2
Tin	Tetragonal	$4/mmm$	10^{-4}	4.07	1
			1	1.66	7.54
Aragonite $l_2/l_1 = 0.1$	Orthorhombic	mmm	10^{-4}	3.73	1
			1	1.81	1.15
Aragonite $l_2/l_1 = 1$	Orthorhombic	mmm	10^{-4}	3.73	1
			1	1.35	15.1
Aragonite $l_2/l_1 = 10$	Orthorhombic	mmm	10^{-4}	3.73	1
			1	1.25	819

For future work, non-centrosymmetric materials will be studied. In non-centrosymmetric materials, there is coupling between force stress - curvatures and couple stress - strains. This will need some changes in the formulations. Also an extension of current research can be studied for 3D structures, where a full constitutive matrix with more independent parameters will come into play. For such analysis, it is anticipated that alternative elements, such as those from the Nédélec family, may be useful. In any case, careful physical experiments are needed to validate the theory and to establish the couple stress material parameters. The effect of classical and size-dependent piezo-electricity and

other multiphysics quantities on anisotropic materials can also be developed based on the mixed variational approach introduced here.

References

Apostolakis, G., Dargush, G.F., 2011. Mixed lagrangian formulation for linear thermoelastic response of structures. Journal of Engineering Mechanics 138, 508–518.

Apostolakis, G., Dargush, G.F., 2013. Variational methods in irreversible thermoelasticity: theoretical developments and minimum principles for the discrete form. Acta Mechanica 224, 2065–2088.

Chakravarty, S., Hadjesfandiari, A.R., Dargush, G.F., 2017. A penalty-based finite element framework for couple stress elasticity. Finite Elements in Analysis and Design 130, 65–79.

Chen, S., Wang, T., 2001. Strain gradient theory with couple stress for crystalline solids. European Journal of Mechanics-A/Solids 20, 739–756.

Chen, S., Wang, T., 2002. Finite element solutions for plane strain mode i crack with strain gradient effects. International journal of solids and structures 39, 1241–1257.

Cosserat, E., Cosserat, F., 1909. Théorie des corps déformables (Theory of deformable bodies) .

Darrall, B.T., Dargush, G.F., Hadjesfandiari, A.R., 2014. Finite element lagrange multiplier formulation for size-dependent skew-symmetric couple-stress planar elasticity. Acta Mechanica 225, 195–212.

Dehkordi, S.F., Beni, Y.T., 2017. Electro-mechanical free vibration of single-walled piezoelectric/flexoelectric nano cones using consistent couple stress theory. International Journal of Mechanical Sciences 128, 125–139.

Deng, G., Dargush, G.F., 2017. Mixed lagrangian formulation for size-dependent couple stress elastodynamic and natural frequency analyses. International Journal for Numerical Methods in Engineering 109, 809–836.

Eringen, A.C., 1999. Theory of micropolar elasticity, in: Microcontinuum field theories. Springer, pp. 101–248.

Ghosh, S., Liu, Y., 1995. Voronoi cell finite element model based on micropolar theory of thermoelasticity for heterogeneous materials. International journal for numerical methods in engineering 38, 1361–1398.

Hadjesfandiari, A., Dargush, G., 2012. Boundary element formulation for plane problems in couple stress elasticity. International Journal for Numerical Methods in Engineering 89, 618–636.

Hadjesfandiari, A.R., Dargush, G.F., 2011. Couple stress theory for solids. International Journal of Solids and Structures 48, 2496–2510.

Hu, H.C., 1955. On some variational principles in the theory of elasticity and the theory of plasticity .

Huang, F.Y., Yan, B.H., Yan, J.L., Yang, D.U., 2000. Bending analysis of micropolar elastic beam using a 3-d finite element method. International journal of engineering science 38, 275–286.

Koiter, W., 1964. Couple stresses in the theory of elasticity. Proc. Koninklijke Nederl. Akaad. van Wetensch 67.

Lata, P., Kaur, H., 2019a. Axisymmetric deformation in transversely isotropic thermoelastic medium using new modified couple stress theory. Coupled Systems Mechanics 8, 501–522.

Lata, P., Kaur, H., 2019b. Deformation in transversely isotropic thermoelastic medium using new modified couple stress theory in frequency domain. Geomechanics and Engineering 19, 369.

Lavan, O., 2010. Dynamic analysis of gap closing and contact in the mixed lagrangian framework: toward progressive collapse prediction. Journal of engineering mechanics 136, 979–986.

Lavan, O., Sivaselvan, M., Reinhorn, A., Dargush, G., 2009. Progressive collapse analysis through strength degradation and fracture in the mixed lagrangian formulation. Earthquake Engineering & Structural Dynamics 38, 1483–1504.

Lazar, M., Maugin, G.A., Aifantis, E.C., 2005. On dislocations in a special class of generalized elasticity. physica status solidi (b) 242, 2365–2390.

Li, A., Zhou, S., Zhou, S., Wang, B., 2014. Size-dependent analysis of a three-layer microbeam including electromechanical coupling. Composite Structures 116, 120–127.

Li, L., Xie, S., 2004. Finite element method for linear micropolar elasticity and numerical study of some scale effects phenomena in mems. International Journal of Mechanical Sciences 46, 1571–1587.

Ma, H., Gao, X.L., Reddy, J., 2008. A microstructure-dependent timoshenko beam model based on a modified couple stress theory. Journal of the Mechanics and Physics of Solids 56, 3379–3391.

Mindlin, R., Eshel, N., 1968. On first strain-gradient theories in linear elasticity. International Journal of Solids and Structures 4, 109–124.

Mindlin, R., Tiersten, H., 1962. Effects of couple-stresses in linear elasticity. Archive for Rational Mechanics and analysis 11, 415–448.

Mindlin, R.D., 1964. Micro-structure in linear elasticity. Archive for Rational Mechanics and Analysis 16, 51–78.

Mohammadi, K., Mahinzare, M., Rajabpour, A., Ghadiri, M., 2017. Comparison of modeling a conical nanotube resting on the winkler elastic foundation based on the modified couple stress theory and molecular dynamics simulation. The European Physical Journal Plus 132, 115.

Nowacki, W., 1986. Theory of asymmetric elasticity. Pergamon Press, Headington Hill Hall, Oxford OX 3 0 BW, UK, 1986. .

Nye, J.F., 1985. Physical properties of crystals: their representation by tensors and matrices. Oxford university press.

Patel, B.N., Pandit, D., Srinivasan, S.M., 2017. A simplified moment-curvature based approach for large deflection analysis of micro-beams using the consistent couple stress theory. European Journal of Mechanics-A/Solids 66, 45–54.

Providas, E., Kattis, M., 2002. Finite element method in plane cosserat elasticity. Computers & structures 80, 2059–2069.

Reddy, J., 2011. Microstructure-dependent couple stress theories of functionally graded beams. Journal of the Mechanics and Physics of Solids 59, 2382–2399.

Reissner, E., 1950. On a variational theorem in elasticity. Studies in Applied Mathematics 29, 90–95.

Riahi, A., Curran, J.H., 2009. Full 3d finite element cosserat formulation with application in layered structures. Applied mathematical modelling 33, 3450–3464.

Romanoff, J., Reddy, J., 2014. Experimental validation of the modified couple stress timoshenko beam theory for web-core sandwich panels. Composite Structures 111, 130–137.

Sachio, N., Benedict, R., Lakes, R., 1984. Finite element method for orthotropic micropolar elasticity. International Journal of Engineering Science 22, 319–330.

Sharbati, E., Naghdabadi, R., 2006. Computational aspects of the cosserat finite element analysis of localization phenomena. Computational materials science 38, 303–315.

Simmons, G., Wang, H., et al., 1971. Single crystal elastic constants and calculated aggregate properties .

Sivaselvan, M.V., Lavan, O., Dargush, G.F., Kurino, H., Hyodo, Y., Fukuda, R., Sato, K., Apostolakis, G., Reinhorn, A.M., 2009. Numerical collapse simulation of large-scale structural systems using an optimization-based algorithm. Earthquake Engineering & Structural Dynamics 38, 655–677.

Sivaselvan, M.V., Reinhorn, A.M., 2006. Lagrangian approach to structural collapse simulation. Journal of Engineering mechanics 132, 795–805.

Subramaniam, C., Mondal, P.K., 2020. Effect of couple stresses on the rheology and dynamics of linear maxwell viscoelastic fluids. Physics of Fluids 32, 013108.

Tan, Z.Q., Chen, Y.C., 2019. Size-dependent electro-thermo-mechanical analysis of multilayer cantilever microactuators by joule heating using the modified couple stress theory. Composites Part B: Engineering 161, 183–189.

Toupin, R.A., 1962. Elastic materials with couple-stresses. Archive for Rational Mechanics and Analysis 11, 385–414.

Voigt, W., 1887. Theoretische Studien über die Elasticitätsverhältnisse der Krystalle(Theoretical studies on the elasticity relationships of crystals). Abhandlungen der Königlichen Gesellschaft der Wissenschaften in Göttingen, Dieterichsche Verlags-Buchhandlung.

Washizu, K., 1975. Variational methods in elasticity and plasticity. Pergamon press.

Wei, Y., 2006. A new finite element method for strain gradient theories and applications to fracture analyses. European Journal of Mechanics-A/Solids 25, 897–913.

Wood, R., 1988. Finite element analysis of plane couple-stress problems using first order stress functions. International journal for numerical methods in engineering 26, 489–509.

Yang, F., Chong, A., Lam, D.C.C., Tong, P., 2002. Couple stress based strain gradient theory for elasticity. International Journal of Solids and Structures 39, 2731–2743.